HINT1 Aggravates Aortic Aneurysm by Targeting ITGA6/FAK Axis in Vascular Smooth Muscle Cells

Authors

Yan Zhang[1]†, Wencheng Wu [1]†, Xuehui Yang[1]†, Shanshan Luo[1]†, Xiaoqian Wang[1],Qiang Da[1], Ke Yan[1], Lulu Hu[1], Shixiu Sun[1], Xiaolong Du[4], Xiaoqiang Li[4], Zhijian Han[5], Feng Chen[1,6], Aihua Gu[7], Liansheng Wang[8], Zhiren Zhang[2], Bo Yu[9], Chenghui Yan[2,10], Yaling Han[2,10], Yi Han[3]*, Liping, Xie [1]*, Yong Ji [1,2]*

Affiliations

[1]Key Laboratory of Drug Targets and Translational Medicine for Cardio-cerebrovascular Diseases；Key Laboratory of Targeted Intervention of Cardiovascular Disease; Collaborative Innovation Center for Cardiovascular Disease Translational Medicine; Medical Basic Research Innovation Center for Cardiovascular and Cerebrovascular Diseases, Ministry of Education, Nanjing Medical University, Nanjing, Jiangsu, China;

[2]State Key Laboratory of Frigid Zone Cardiovascular Diseases (SKLFZCD), Harbin Medical University, Harbin, Heilongjiang, PR China;

[3]Critical Care Department, The Second Affiliated Hospital of Harbin Medical University;

[4]Department of Vascular Surgery, The Affiliated Nanjing Drum Tower Hospital, Nanjing University Medical School, Nanjing, China;

[5]Department of Urology, First Affiliated Hospital of Nanjing Medical University, Nanjing, China;

[6]Departments of Forensic Medicine, Nanjing Medical University, Nanjing, China;

[7]School of Public Health, Nanjing Medical University, Nanjing, China;

[8]Departments of Cardiology, the First Affiliated Hospital of Nanjing Medical University, Nanjing, China;

[9]Department of Cardiology, The 2nd Affiliated Hospital of Harbin Medical University, The Key Laboratory of Myocardial Ischemia, Ministry of Education, Harbin Medical University, Heilongjiang, China.

[10]Cardiovascular Research Institute and Department of Cardiology, General Hospital of Northern Theater Command, Shenyang, China.

†These authors contributed equally to this work.

***Corresponding author:**

*Yong Ji, MD, PhD, Tel: 0451-86615600; Fax: 0451-86661458;

Address: Harbin Medical University, 157 Baojian Rd, Nangang District, Harbin, Heilongjiang, 150081, China.

E-mail: yongji@njmu.edu.cn; yongji@hrbmu.edu.cn

*Liping Xie, MD, PhD. Tel: +86-25-86869331;

Address: Nanjing Medical University,101 Longmian Ave, Jiangning District, Nanjing, Jiangsu, 211166, China.

E-mail: lipingxie@njmu.edu.cn

*Yi Han, MD, PhD. Tel: +86-451-86605052;

Address: The Second Affiliated Hospital of Harbin Medical University, 246 Xuefu Rd, Nangang District, Harbin, Heilongjiang, 150086, China

E-mail: yihan@hrbmu.edu.cn; hanyi@jsph.org.cn

Conflict of interest: The authors have declared that no conflict of interest exists.

Abstract

Aortic aneurysm is a high-risk cardiovascular disease without effective cure. Vascular Smooth Muscle Cell (VSMC) phenotypic switching is a key step in the pathogenesis of aortic aneurysm. Here, we revealed the role of histidine triad nucleotide-binding protein 1 (HINT1) in aortic aneurysm. HINT1 was upregulated both in aortic tissue from patients with aortic aneurysm and Ang II-induced aortic aneurysm mice. VSMC-specific HINT1 deletion alleviated aortic aneurysm via preventing VSMC phenotypic switching. With the stimulation of pathological factors, the increased nuclear translocation of HINT1 mediated by nucleoporin 98 (Nup98) promoted the interaction between HINT1 and transcription factor AP-2 alpha (TFAP2A) and further triggered the transcription of integrin alpha 6 (ITGA6) mediated by TFAP2A, and consequently activated the downstream focal adhesion kinase (FAK)/STAT3 signal pathway, leading to aggravation of VSMC phenotypic switching and aortic aneurysm. Importantly, Defactinib treatment was demonstrated to limit aortic aneurysm development by inhibiting the FAK signal pathway. Thus, HINT1/ITGA6/FAK axis emerges as potential therapeutic strategies in aortic aneurysm.

Introduction

Aortic aneurysm is a life-threatening cardiovascular event that is characterized by permanent dilatation of aorta and an extremely high mortality rate in the event of rupture (1, 2). Aortic aneurysm is associated with high mortality, but neither predictive risk factors nor medical treatments have been established for aortic aneurysm. Endovascular surgical repair remains the main treatment option for aortic aneurysm (3). Consequently, decoding the molecular mechanism involved in aortic aneurysm is critical for identifying potential pharmacological interventions.

Compelling evidence has shown that VSMC phenotypic switching is a key step in the pathogenesis of aortic aneurysm (1, 4). Single-cell RNA sequencing and lineage tracing analyses revealed that VSMC phenotypic switching plays an essential role in the pathogenesis of aortic aneurysms (5-7). VSMCs are highly plastic, and they can exist in either contractile or synthetic phenotype in response to various stimuli, including micro-environmental cues (8, 9). The contractile phenotype of VSMCs is marked by high expression of calponin (CNN1), α-smooth muscle actin (ACTA2), and SM22 (TAGLN), which are essential for cellular contraction, modulation of vascular tone, blood pressure homeostasis, and blood flow redistribution. Synthetic VSMCs can markedly increase their capacity to proliferate and migrate and promote the synthesis of elastolytic and pro-inflammatory factors (10). This phenotypic switching results in extracellular matrix degradation and aortic wall weakening, which ultimately renders the aorta prone to rupture and aortic aneurysm progression (11, 12). However, molecular mechanisms governing VSMC phenotypic switching during the development of aortic aneurysm remain incompletely understood.

HINT1 (histidine triad nucleotide-binding protein 1) is a highly conserved protein that belongs to the histidine triad superfamily, members of which contain the His-X-His-X-His-X motif (where X is a hydrophobic amino acid) (13). Recent studies suggest that HINT1 plays important roles in diverse neuropsychiatric diseases, including schizophrenia, mood disorders, drug addiction, and inherited peripheral neuropathies(14, 15). Loss of HINT1 increases susceptibility to carcinogenesis in mice, suggesting a role as a tumor suppressor (16, 17). HINT1 is located in both cytoplasm and the nucleus (18, 19). Our previous study has demonstrated that HINT1 in cardiomyocytes protects from cardio hypertrophy as an important signal transduction molecule (20). However, the roles of HINT1 in VSMCs and aortic aneurysm have not been addressed.

In this study, by using animal and cell models, we found that HINT1 in VSMCs promoted VSMC phenotypic switching and aggravated Ang II-induced aortic aneurysm in mice. Further, we identified ITGA6 as a target of HINT1 that contributed to VSMC phenotypic switching through activating the FAK/STAT3 signal pathway. Mechanically, under the stimulation of pathological factors, the nuclear translocation of HINT1 mediated by Nup98 increases significantly and HINT1 directly binds to TFAP2A, upregulating the transcription of ITGA6 mediated by TFAP2A and leading to activated FAK-STAT3 signal pathway, and further resulting in aggravating VSMC phenotypic switching. Defactinib, an inhibitor of FAK, significantly limited aortic aneurysm progression in mice by targeting ITGA6/FAK axis.

Results

Increased HINT1 expression in the vascular smooth muscle is associated with the occurrence of aortic aneurysm.

To underling the mechanism of aortic aneurysm, we analyzed two RNA sequencing datasets (GSE26155 and GSE57691) and one proteomics dataset (PXD032293), in which differently expressed genes/proteins were identified in aortic samples from patients with aortic aneurysm and non-aortic aneurysm controls. We identified 15 differently expressed genes/proteins (fold change >1.5, FDR<0.05) which overlapped in the above 3 databases (Figure 1A). Importantly, we found HINT1, which was demonstrated to protect against cardiac hypertrophy in our previous study (20), as a member of the 15 identified genes/proteins, suggesting that it may be involved in aortic aneurysm. Next, we went on to clarify the role of HINT1 in the aortic aneurysm. As shown in Figure 1B and Figure 1C, the protein and mRNA levels of *HINT1* were markedly higher in aorta samples from aortic aneurysm patients than that in normal aorta samples from donors. Moreover, immunofluorescence staining also revealed increased HINT1 in aorta from aortic aneurysm patients than that from control subjects (Figure 1D). Meanwhile, we observed that HINT1 was colocalized with α-smooth muscle actin (α-SMA) in aorta samples (Figure 1D), which suggests that HINT1 is mainly located in VSMCs. Subcutaneous administration of Ang II by a mini pump was used to induce aortic aneurysm in *Apoe*$^{-/-}$ mice. An increase in protein (Figure 1E) and mRNA level (Figure 1F) of *Hint1* were observed in the suprarenal abdominal aortas of *Apoe*$^{-/-}$ mice infused with Ang II compared with controls. Furthermore, we observed a marked increase of HINT1 at various timepoints (3, 7, 28 days) after Ang II infusion

(Supplemental Figure 1A). In addition, we found that Ang II treatment resulted in marked increased HINT1 in mouse aortic smooth muscle cells (MASMCs), human aortic smooth muscle cells (HASMCs), and rat aortic smooth muscle cells (RASMCs) (Figure 1G-H), while it did not affect HINT1 expression in mouse aortic endothelial cells (ECs) (Supplemental Figure 1B-C) and mouse bone marrow derived macrophages (BMDMs) (Supplemental Figure 1D-E), implying an important role of HINT1 in VSMCs in aortic aneurysm. Taken together, upregulation of HINT1 expression in VSMCs is correlated with aortic aneurysm in both humans and mice, suggesting that HINT1 may play an important role in the progression of aortic aneurysm.

VSMC specific knockout of Hint1 alleviates angiotensin II (Ang II)-induced aortic aneurysms in vivo.

To determine the role of HINT1 in VSMCs in the progression of aortic aneurysm, we constructed VSMC-specific *Hint1* knockout mice (*Hint1*^{SMKO} mice) by crossing *Hint1*$^{flox/flox}$ (*Hint1*$^{f/f}$) mice with *Tagln*-Cre mice. Western blotting and q-PCR confirmed the deletion of *Hint1* in VSMCs isolated from *Hint1*^{SMKO} mice (Supplemental Figure 2A-B). Next, *Hint1*^{SMKO} mice were crossed with *Apoe*$^{-/-}$ mice. We then induced aortic aneurysm in *Apoe*$^{-/-}$/*Hint1*^{SMKO} mice and *Apoe*$^{-/-}$/*Hint1*$^{flox/flox}$ littermates by subcutaneous infusion of Ang II for 4 weeks. Gross examination showed lower luminal expansion in suprarenal region of the abdominal aorta of *Apoe*$^{-/-}$/*Hint1*^{SMKO} mice than *Apoe*$^{-/-}$/*Hint1*$^{flox/flox}$ mice induced with Ang II (Figure 2A). Notably, there were no blood pressure (BP) differences between the two groups, suggesting that the effects of HINT1

in VSMCs are not related to BP (Supplemental Figure 2C). The incidence of aortic aneurysm reduced from 81.2% in *Apoe*$^{-/-}$/*Hint1*$^{flox/flox}$ mice to 18.7% in *Apoe*$^{-/-}$/*Hint1*^{SMKO} mice infused with Ang II (Figure 2B). The aortic rupture rate in *Apoe*$^{-/-}$/*Hint1*$^{flox/flox}$ mice was 18.7%, while that was 6.2% in *Apoe*$^{-/-}$/ *Hint1*^{SMKO} mice infused with Ang II (Supplemental Figure 2D). As determined by transabdominal ultrasound imaging (Figure 2C) and post-mortem measurement (Supplemental Figure 2E), *Hint1* deficiency in VSMCs markedly decreased aortic diameter in *Apoe*$^{-/-}$/ *Hint1*^{SMKO} mice infused with Ang II. Morphologically, histological analysis results revealed that VSMC-specific *Hint1* knockout mitigated arterial wall thickening and reduced elastic fiber degradation and collagen deposition in Ang II-administered mouse suprarenal abdominal aortas (Figure 2D). Moreover, we found that the activity of matrix metalloproteinase decreased in the aortas of the *Apoe*$^{-/-}$/*Hint1*^{SMKO} mice by in situ zymography (Figure 2E). Furthermore, we observed markedly increased α-SMA in suprarenal abdominal aorta from *Apoe*$^{-/-}$/*Hint1*^{SMKO} mice infused with Ang II by immunofluorescent staining (Figure 2F). Consistently, we found increased contractile proteins (α-SMA and SM22) and decreased synthetic proteins (Vimentin) in the suprarenal abdominal aorta from Ang II infused *Apoe*$^{-/-}$/*Hint1*^{SMKO} mice (Figure 2G). Meanwhile, q-PCR of suprarenal abdominal aorta revealed that knockout of *Hint1* in VSMCs resulted in a marked increase of contractile genes including *Tagln*, *Acta2* and *Cnn1*, whereas the expression of synthetic genes including *Klf4*, *Opn* and *Mhy10* was reduced (Figure 2H), which suggests that HINT1 promotes vascular smooth muscle cell phenotypic conversion.

Hint1 deficiency represses the phenotypic switching of VSMCs.

Next, we investigated whether HINT1 triggers VSMC phenotypic switching in vitro. PDGF-BB is a recognized factor to induce VSMC phenotypic switching in vitro when Ang II is infused to induce aortic aneurysms in vivo (21, 22). We observed a marked upregulation of HINT1 in PDGF-BB induced RASMCs, HASMCs and MASMCs by q-PCR (Supplemental Figure 3A) and western Blot (Supplemental Figure 3B). As shown in Supplemental Figure 3C, under stimulation of PDGF-BB, primary aortic VSMCs from *Hint1*$^{-/-}$ mice showed increased contractile proteins (α-SMA and SM22) and decreased synthetic proteins (Vimentin) than controls, which suggests that deficiency of *Hint1* disrupts phenotypic transformation of VSMC in vitro. Meanwhile, q-PCR revealed that deficiency of *Hint1* in mouse VSMCs resulted in a marked increase of contractile genes including *Tagln*, *Acta2* and *Cnn1* while the expression of synthetic genes including *Klf4*, *Opn* and *Mhy10* was decreased (Supplemental Figure 3D). Moreover, phalloidin staining revealed that *Hint1* deficiency inhibited the microfilaments remodeling and prevented morphological changes of VSMCs from a spindle-like contractile phenotype to a polygonal synthetic phenotype (Supplemental Figure 3E). Meanwhile, we demonstrated that knockdown of *HINT1* in HASMCs by siRNA reversed PDGF-BB-triggered VSMC phenotypic alteration from contractile to synthetic phenotypes (Supplemental Figure 3F-G). A similar phenomenon was also observed by phalloidin staining (Supplemental Figure 3H). In addition, we also confirmed that HINT1 promoted Ang II-induced VSMC phenotypic switching in vitro

(Supplemental Figure 4). Collectively, we demonstrated that *Hint1* deficiency maintains the contractile phenotype of VSMCs.

HINT1 effects on phenotypic switching of VSMCs via targeting integrin α6.

To identify the downstream targets of HINT1 in phenotypic switching of VSMCs, we conducted RNA-sequencing analysis (GSE 289426) to evaluate transcriptomic changes caused by deficiency of HINT1 in primary mouse aortic VSMCs stimulated with PDGF-BB. A total of 168 upregulated and 165 downregulated genes (fold change>1.5, FDR<0.05) were identified in VSMCs from *Hint1*$^{-/-}$ mice simulated with PDGF-BB compared with WT VSMCs. Kyoto Encyclopedia of Genes and Genomes (KEGG) pathway and enrichment analysis revealed that deficiency of HINT1 in VSMCs stimulated with PDGF-BB was related to four pathways, including PI3K-AKT signaling pathway, ECM-receptor interaction, regulation of actin cytoskeleton, and focal adhesion (Figure 3A). We screened four genes including *Integrin α6* (*Itga6*), *Integrin α7* (*Itga7*), *Integrin α8* (*Itga8*) and *Integrin β8* (*Itgb8*). These genes were enriched in the above four pathways, which suggests that they may participate in phenotypic switching of VSMCs mediated by HINT1 (Figure 3B). Next, q-PCR was performed to verify the expression level of these genes in VSMCs from WT and *Hint1*$^{-/-}$ mice treated with PDGF-BB. We demonstrated that *Hint1* deficiency caused reduced *Itga6* but had no effect on *Itga7*, *Itga8* or *Itgb8*, with the treatment of PDGF-BB or Ang II (Figure 3C, Supplemental Figure 5A). Furthermore, we confirmed that either *Hint1* deficiency in MASMCs (Figure 3D-E, Supplemental Figure 5B-C) or *HINT1*

knockdown in HASMCs (Figure 3F-G, Supplemental Figure 5D-E) resulted in a marked decrease of ITGA6, with the treatment of PDGF-BB or Ang II. Meanwhile, we observed reduced ITGA6 in the aorta from *Apoe*$^{-/-}$/*Hint1*^{SMKO} mice compared with that in the aorta from *Apoe*$^{-/-}$/*Hint1*$^{flox/flox}$ mice infused with Ang II both by q-PCR (Figure 3H), Western blot (Figure 3I) and immunofluorescence (Figure 3J). Collectively, these results indicate that HINT1 promotes phenotypic transformation of VSMCs via targeting ITGA6.

ITGA6 promotes VSMC phenotypic switching.

To explore the role of ITGA6 in phenotypic switching of VSMCs, we evaluated the expression of ITGA6 in VSMCs. We found increased ITGA6 in aorta samples from aortic aneurysm patients than that in normal aorta samples from donors by western blot (Figure 4A) and q-PCR (Figure 4B). In addition, ITGA6 was upregulated in Ang-II infused *Apoe*$^{-/-}$ mice (Supplemental Figure 6A-C). Besides, we also found an upregulation of ITGA6 in PDGF-BB-induced HASMCs, RASMCs and MASMCs (Supplemental Figure 6D-E). Moreover, we found that knockdown of *ITGA6* in VSMCs showed increased contractile proteins and decreased synthetic proteins (Supplemental Figure 6F-6G), which suggests that knockdown of *ITGA6* prevents phenotypic switching of VSMCs. In addition, phalloidin staining revealed that knockdown of *Itga6* inhibited the microfilaments remodeling and prevented morphological changes of VSMCs from a spindle-like contractile phenotype to a polygonal synthetic phenotype (Supplemental Figure 6H).

ITGA6 in VSMCs aggravates Ang II-induced aortic aneurysm.

To clarify the role of ITGA6 in aortic aneurysm, we injected lentivirus vector encoding negative shRNA control (Lenti-sh*NC*) or lentivirus vector encoding shRNA targeting *Itga6* (Lenti-sh*Itga6*) with 2 reverse loxP sites, which can be recognized by Cre recombinase. These lentiviruses were injected into *Apoe*$^{-/-}$/*Tagln-Cre* mice through the tail vein to specifically downregulate the *Itga6* level in VSMCs. Two weeks later, these mice were infused with Ang II or saline for 4 weeks (Supplemental Figure 7A) and ITGA6 level in the mouse aorta was confirmed downregulated (Supplemental Figure 7B). Gross examination showed lower luminal expansion in suprarenal region of the abdominal aorta of Ang II infused *Apoe*$^{-/-}$/*Tagln-Cre* mice in which *Itga6* was reduced in VSMCs (Figure 4C). In addition, we showed that the knock down of *Itga6* had no effect on blood pressure (BP), suggesting that the effects of ITGA6 on aortic aneurysm are not related to BP control (Supplemental Figure 7C). Silence of *Itga6* resulted in decreased incidence of aortic aneurysm (Figure 4D), reduced aortic diameter (Figure 4E, Supplemental Figure 7D). The aortic rupture rate in Lenti-sh*NC* mice was 27.2%, while that was 9.0% in Lenti-sh*Itga6* mice infused with Ang II (Supplemental Figure 7E). Morphologically, histological analysis results revealed that knockdown of *Itga6* in VSMCs mitigated arterial wall thickening and reduced elastic fiber degradation and collagen deposition in Ang II-administered mouse suprarenal abdominal aortas (Figure 4F). Moreover, we demonstrated that downregulation of *Itga6* decreased the activity of matrix metalloproteinase (Figure 4G) and increased α-SMA (Figure 4H) in aortic tissue. In addition, western blot (Figure 4I) and q-PCR (Supplemental Figure 7F) revealed that

knockdown of *Itga6* led to an increase of contractile markers and a decrease of synthetic markers in the suprarenal abdominal aorta from Ang II infused *Apoe*$^{-/-}$/*Tagln-Cre* mice, which suggests that ITGA6 promotes VSMC phenotypic switching. Taken together, these results indicate that ITGA6 in VSMCs causes vascular smooth muscle cell phenotypic switching and aggravates aortic aneurysms in vivo.

Impact of HINT1 on aortic aneurysm relies on its regulation of ITGA6.

To evaluate whether the effects of HINT1 on aortic aneurysm rely on its regulation of ITGA6 in vivo, we injected lentivirus vectors encoding control (Lenti-*Ctrl*) or *Itga6* (Lenti-*Itga6*) with reverse loxP sites, which can be recognized by Cre recombinase, into *Apoe*$^{-/-}$/*Hint1*^{SMKO} and *Apoe*$^{-/-}$/ *Hint1*$^{flox/flox}$ littermates through tail vein to specifically overexpress *Itga6* in VSMCs. Two weeks later, these mice were infused with Ang II or saline for 4 weeks (Supplemental Figure 8A) and the BP of mice were detected (Supplemental Figure 8B). As shown in Figure 5A, knock out of *Hint1* in VSMCs alleviated aortic aneurysm, and simultaneous overexpression of *Itga6* reversed this protective effect. Consistent with these findings, the incidence of aortic aneurysm (Figure 5B) and aortic diameter (Figure 5C, Supplemental Figure 8C) were substantially decreased in the *Apoe*$^{-/-}$/*Hint1*^{SMKO} mice, which were reversed by injection of Lenti-*Itga6*. We observed reduced aortic rupture rate caused by deficiency of *Hint1*, however, these beneficial effects were eliminated by overexpression of *Itga6* (Supplemental Figure 8D). Deficiency of *Hint1* in VSMCs reduced the elevation of aortic medial thickness, fragmentation of elastic fibers, deposition of collagen in the

suprarenal aorta; however, these beneficial effects were eliminated by overexpression of *Itga6* (Figure 5D). Meanwhile, VSMC-specific knockout of *Hint1* reduced MMP activity and increased α-SMA expression in the suprarenal aorta while this phenomenon was diminished by overexpression of *Itga6* (Figure 5E-F). Furthermore, overexpression of *Itga6* reversed the inhibition of deficiency of *Hint1* in VSMC phenotypic switching (Figure 5G and Supplemental Figure 8E).

To further confirm that the regulatory effects of HINT1 on VSMC phenotypic switching are ITGA6-dependent, *ITGA6* was overexpressed by lentivirus transfection when *HINT1* was silenced by siRNA in VSMCs. Western blotting and q-PCR showed that *ITGA6* overexpression reversed the reduction of phenotypic switching of VSMCs induced by *HINT1* knockdown (Supplemental Figure 8F-G). We observed consistent results through the phalloidin staining (Supplemental Figure 8H). These findings demonstrated that HINT1 promoted phenotypic switching of VSMCs via upregulating ITGA6 expression in vitro. Taken together, these results suggest that HINT1 in VSMC aggravates aortic aneurysm by increasing the expression of ITGA6.

HINT1 regulates ITGA6 transcription via its interaction with TFAP2A.

To further address how HINT1 regulates ITGA6 transcription and expression, UCSC and JASPAR databases were combined and employed to identify transcription factors of *ITGA6*. Meanwhile, the transcription factors which are regulated by HINT1 were identified by the RNA-seq as we performed above in Figure 3A. After cross-comparing these two datasets, we identified three transcription factors, including TCF21, TFAP2A

and AR, which may be the potential transcription factors for *ITGA6* and regulated by HINT1 (Figure 6A). Luciferase reporter assays showed that TFAP2A may be the transcription factor for *ITGA6* but not TCF21 or AR (Supplemental Figure 9A). Further, we observed reduced ITGA6 when *TFAP2A* was knockdown in HASMCs treated with PDGF-BB or Ang II (Figure 6B-C, Supplemental Figure 9B-C). Luciferase reporter assays (Figure 6D) and chromatin immunoprecipitation (ChIP) assay (Supplemental Figure 9D) verified the binding of TFAP2A to the promoter of *ITGA6* and PDGF-BB stimulation increased this binding. Chromatin immunoprecipitation assay revealed that the knockdown of *Hint1* reduced PDGF-BB/Ang II-induced binding of TFAP2A to the *Itga6* promoter (Figure 6E, Supplemental Figure 9E). Luciferase reporter assays also demonstrated that overexpression of *HINT1* promoted *ITGA6* transcription mediated by TFAP2A in HEK293T (human embryonic kidney 293T) cells (Figure 6F). Next, we went on to uncover the motifs of the promoter of *ITGA6* that TFAP2A binds to. According to the predicted binding sites of TFAP2A in the *ITGA6* promoter from JASPAR library, WT and mutations (MUT1, MUT2, MUT3, MUT4, MUT5) of *ITGA6* promoter-firefly luciferase reporter plasmids were constructed and transfected into HEK293T cells. Luciferase reporter assays showed that TFAP2A did not stimulate the activity of the MUT5-*ITGA6* promoter. These results indicate the promoter region between -230 to -109 base pair is the TFAP2A binding site (Figure 6G).

Next, we aimed to investigate the mechanism by which HINT1 regulates *ITGA6* transcription via TFAP2A. As a transcription co-factor, HINT1 has been reported to regulate a series of transcription factors by interacting with them, including USF2,

MITF, and β-catenin (18, 19). We speculated that HINT1 can interact with TFAP2A and further regulate its activity as a transcription factor. To test our hypothesis, co-immunoprecipitation (Figure 6H) and immunofluorescence (Figure 6I) were performed. When both Flag-tagged TFAP2A and HA-tagged HINT1 were co-transfected into HEK293T cells, Co-IP with Flag or HA antibody showed that Flag-TFAP2A interacted with HA-HINT1 in cells (Figure 6J and Supplemental Figure 9F). Next, purified proteins of HINT1 and GST-TFAP2A were synthesized, and we observed that the two proteins could directly interact with each other in vitro (Figure 6K and Supplemental Figure 9G), which suggests that there is a direct interaction between HINT1 and TFAP2A. Furthermore, we found that PDGF-BB/Ang II stimulation increased the interaction between TFAP2A and HINT1 in HASMCs by Co-IP (Figure 6L and Supplemental Figure 9H) and immunofluorescence co-localization (Supplemental Figure 9I). Taken together, we demonstrated that HINT1 promotes ITGA6 transcription and expression via enhanced its interaction with TFAP2A.

HINT1 enhances the interaction with TFAP2A by its increased nuclear translocation mediated by Nup98 under stimulation of PDGF-BB.

Next, we wondered the reason why the interaction between HINT1 and TFAP2A was increased under pathological stimulus, which led to upregulated ITGA6 transcription mediated by TFAP2A. Given that TFAP2A is mostly located in nucleus as we observed and previously reported (23), we speculated that nuclear translocation of HINT1 is increased under stimulation of PDGF-BB, which leads to more interaction and co-

localization of HINT1 and TFAP2A. As expected, we identified more nuclear translocation of HINT1 in PDGF-BB treated HASMCs by western blot (Supplemental Figure 10A) and immunofluorescence (Supplemental Figure 10B). To clarify why the nuclear translocation of HINT1 was increased under stimulation of PDGF-BB, the interacting proteins of HINT1 were pulled down by co-immunoprecipitation using the antibody of HINT1 and sent to be identified by mass spectrum (MS). The MS results showed that NUP98, an important component of the nuclear pore complex, could interact with HINT1 (Supplemental Figure 10C). Nuclear pore complex is a large protein channel in the nuclear membrane of cells that is responsible for the transport of substances between the nucleus and cytoplasm (24, 25). The interaction of endogenous HINT1 and NUP98 was confirmed by Co-IP in RASMCs (Supplemental Figure 10D) and HASMCs (Supplemental Figure 10E). Furthermore, we found that the knockdown of *NUP98* by siRNA reduced the nuclear translocation of HINT1 in PDGF-BB treated HASMCs by western blot (Supplemental Figure 10F). In addition, we observed less interaction between HINT1 and TFAP2A (Supplemental Figure 10G), along with decreased ITGA6 expression (Supplemental Figure 10H-I) and attenuated phenotypic switching of VSMCs when *NUP98* was knocked down in PDGF-BB treated HASMCs (Supplemental Figure 10J-K). Taken together, we demonstrated that HINT1 enhances the interaction with TFAP2A by its increased nuclear translocation mediated by Nup98 under stimulation of PDGF-BB.

ITGA6 exacerbates VSMC phenotypic switching via activating FAK/STAT3 signal pathway.

Next, to investigate the mechanism underlying how ITGA6 impacts on VSMC phenotype switching, protein-protein interaction network of ITGA6 interacting proteins was constructed using the STRING database, and PTK2 was identified as a target that involved with ITGA6 (Supplemental Figure 11A). PTK2 is the gene name of focal adhesion kinase (FAK). Previous study reported that activated FAK could trigger downstream STAT3 signaling pathway (26, 27), which is recognized to promote VSMC phenotype switching (28). So we speculated that ITGA6 affected VSMC phenotype switching via FAK/STAT3 signal pathway. As expected, we observed reduced p-FAK and p-STAT3 level in *ITGA6* knockdown HASMCs (Figure 7A). In addition, a reduced nuclear translocation of STAT3 was confirmed when *ITGA6* was knockdown (Supplemental Figure 11B). Defactinib, an inhibitor of FAK (29), reduced FAK activation, downstream phosphorylation of STAT3 (Supplemental Figure 11C), and nuclear translocation of STAT3 (Supplemental Figure 11D-E). Furthermore, we found that Defactinib could inhibit VSMC phenotypic switching by western blot (Figure 7B) and q-PCR (Supplemental Figure 11F). We further detected that Defactinib treatment inhibited the FAK/STAT3 signal pathway (Supplemental Figure 11G) and nuclear translocation of STAT3 (Supplemental Figure 11H) induced by overexpression of ITGA6. Besides, we observed that overexpression of *ITGA6* promoted VSMC phenotypic switching, and Defactinib treatment attenuated this effect, indicating that ITGA6 aggravates VSMC phenotypic switching via activating FAK signal pathway

(Figure 7C and Supplemental Figure 11I-J). Furthermore, we observed reduced p-FAK in *Hint1* silenced HASMCs (Figure 7D) and Defactinib treatment attenuated VSMC phenotypic switching induced by overexpression of *HINT1*(Figure 7E and Supplemental Figure 11K). Taken together, our findings suggest that ITGA6 aggravates VSMC phenotypic switching via activating the FAK/STAT3 signal pathway.

Pharmacological blockade of FAK activation by Defactinib protects against aortic aneurysm.

Eight-week-old male *Apoe*$^{-/-}$ mice were treated with Defactinib (20 mg/kg/day) daily via intragastric administration, starting at the first day of Ang II infusion and continuing for 28 days (Figure 8A). Treatment with Defactinib resulted in a marked reduction in the aortic diameter (Figure 8B, 8D, Supplemental Figure 12A) and decreased incidence (Figure 8C) of aortic aneurysm compared to controls. *Apoe*$^{-/-}$ mice treated with Defactinib did not cause aortic rupture after the Ang II infusion compared with controls (Supplemental Figure 12B). BP and body weight did not change in *Apoe*$^{-/-}$ mice treated with Defactinib (Supplemental Figure 12C-12D). Hematoxylin & eosin staining revealed a marked reduction in the aortic medial thickness and elastic van Gieson staining showed lower severe fragmentation of elastic fibers in the *Apoe*$^{-/-}$ mice which received Defactinib (Figure 8E). Defactinib treatment caused decreased global MMP activity (Figure 8F) and increased α-SMA expression (Figure 8G) in suprarenal abdominal aorta. We observed alleviated VSMC phenotypic transformation in the suprarenal abdominal aorta of *Apoe*$^{-/-}$ mice which received Defactinib by q-PCR

(Supplemental Figure 12E) and western blotting (Figure 8H). Overall, these data indicate the protective effects of Defactinib against the progression of aortic aneurysm.

Discussion

VSMCs show high plasticity and thus undergo phenotypic switching in response to various pathological stimuli. Recent studies have demonstrated that VSMC phenotypic switching is important in the pathogenesis of a variety of cardiovascular diseases such as atherosclerosis, post injury restenosis and aortic aneurysm/dissection (30-32). In contrast, our understanding of the key factors that regulate VSMC phenotypic switching is limited.

In the present work, we identified the role of HINT1 in VSMC phenotypic switching and the pathogenesis of aortic aneurysm. The contributions included the following: a. Hint1 deficiency in VSMCs alleviates aortic aneurysm formation and progression; b. The driving role of HINT1 in aortic aneurysm is dependent on ITGA6; c. Further mechanistic investigations revealed that ITGA6 promotes aortic aneurysm by activating the downstream FAK/STAT3 signal pathway; d. HINT1 upregulates ITGA6 transcription by interacting with TFAP2A and activating TFAP2A, which is the transcription factor of ITGA6. Taken together, these findings demonstrated that HINT1 promotes VSMC phenotypic switching and aggravates aortic aneurysm in a ITGA6-dependent manner through direct interaction with TFAP2A, which is responsible for the transcriptional activation of ITGA6.

Our previous study identified the role of HINT1 in cardiovascular diseases, in which HINT1 in cardiomyocytes protects from cardiac hypertrophy as an important signal transduction player in cytoplasm (20). Mechanically, HINT1 inhibits PKCβ1 activation by interacting with PKCβ1 and suppresses the downstream HOXA5 expression through

the MEK/ERK/YY1 signal pathway. Other studies have reported that as a transcription cofactor, HINT1 can regulate the activity of a variety of transcription factors, including MITF, NF-KB and USF2 (18, 19). Here, we defined that HINT1 can undergo nuclear translocation as a transcription cofactor of TFAP2A, directly interact with TFAP2A, and increase the transcriptional activity of ITGA6, resulting in the activation of downstream FAK/STAT3 signal pathway and promoting VSMC phenotypic switching and aortic aneurysm.

As a member of the integrins family, integrin α6 (ITGA6) plays important roles in proliferation, migration, and drug resistance. Studies found that downregulation of ITGA6 or specific ITGA6-neutralizing antibodies treatment inhibits acute lymphoblastic leukemia invasion to the central nervous system (33). Increased ITGA6 expression in human endothelial progenitor cells contributes to angiogenesis (34). ITGA6 splice variant regulates proliferation and the Wnt/β-catenin pathway (35). However, the role of ITGA6 in VSMC phenotypic switching or aortic aneurysm has not been elucidated. Our study demonstrated that ITGA6 is a target of HINT1 and promotes VSMC phenotypic switching by coupling with the downstream FAK/STAT3 pathway.

Focal adhesion kinase (FAK) is a non-receptor tyrosine kinase that classically transduces signaling from cell adhesions to regulate multiple biological cellular functions, including cell survival, migration, and invasion of cancer cells (36, 37). FAK is indeed critical in development, tissue regeneration, and wound healing (38). In the vascular system, FAK plays pivotal roles in the vasculature development through the

regulation of SMC recruitment and endothelial vascular network formation (39, 40). Recent studies have revealed that FAK plays a key role in angiogenesis and vascular development (41). FAK signal activation has been proved to be involved with VSMC phenotypic switching (28, 42).

Our current study found that FAK activation mediated by ITGA6 could promote VSMC phenotypic switching. To confirm our findings, Defactinib, an effective inhibitor of FAK, was used. We observed markedly blunt VSMC phenotypic switching and limited aortic aneurysm under treatment of Defactinib. Defactinib is currently being investigated in combination with the PD-1 receptor inhibitor, pembrolizumab, in patients with pancreatic, NSCLC, and mesothelioma cancer (29, 43). Its safety has been confirmed. Based on the effective intervention effect on aortic aneurysms we observed in animal models, Defactinib may have potential for the treatment of aortic aneurysms in the near future.

Methods

Sex as a biological variable

Our study exclusively examined male mice because aortic aneurysm is a sex dimorphic disease and aortic aneurysm exhibits lower female prevalence (44, 45). It is unknown whether the findings are relevant for female mice.

Animals

Hint1$^{flox/flox}$ mice were generated using CRISPR/Cas9 system in Model Animal Research Center of Nanjing Medical University. *Tagln-Cre* mice were purchased from the Model Animal Research Center of Nanjing University. *Hint1*$^{flox/flox}$ mice were crossed with *Tagln-Cre* mice to generate *Hint1*^{SMKO} mice. *Apoe*$^{-/-}$ mice were purchased from GemPharmatech (Nanjing, China). *Apoe*$^{-/-}$ mice were crossed with *Tagln-Cre* mice to generate *Apoe*$^{-/-}$*/Tagln-cre* mice. *Hint1*$^{-/-}$ mice were acquired from Shanghai Key Laboratory of Regulatory Biology, Institute of Biomedical Sciences and School of Life Sciences, East China Normal University. C57BL/6J mice were purchased from Animal Core Facility of Nanjing Medical University. Mice were housed in a pathogen-free and temperature-controlled environment under a 12-hour light/dark cycle. Comparisons were between littermates.

Cell Culture

RASMC were isolated from the aortas of male Sprague-Dawley rats (weight 150-180 g) by collagenase digestion as previously described (30). MASMC were isolated from the thoracic aortas of 4-6 weeks old male WT mice and *Hint1*$^{-/-}$ mice as previously described (46). HASMC (CTCC-001-0065) were purchased from MEISEN CELL

(ZheJiang, China). HEK293T cells were from Cell Bank/Stem Cell Bank, Chinese Academy of Sciences.

Western blot analysis

Cells or tissues were lysed in RIPA lysis buffer (Thermo Fisher Scientific, Waltham, MA) with the addition of protease inhibitor (Roche, Penzberg, Germany) and phosphatase inhibitor (4906845001, Roche, Penzberg, Germany) cocktails. Protein samples were subjected to SDS-PAGE and transferred onto polyvinyl difluoride (PVDF) membranes. After blocking with 5% fat-free milk, the membrane was incubated with indicated primary antibodies at 4 °C overnight. After TBST washing, membranes were incubated with secondary antibody for 1 hour at room temperature. After TBST washing, the bands were obtained by chemiluminescence (GE, USA).

Immunofluorescence Staining

OCT-embedded aortic sections or cultured HASMC or RASMC were fixed with 4% paraformaldehyde for 20 minutes at room temperature. The samples were permeabilized with 0.1% Triton X-100 for 10 minutes, then blocked with 10% BSA for 1 hour. Next, anti-HINT1, anti-α-SMA, anti-ITGA6, anti-TFAP2A or anti-STAT3 antibody was added to the sections or cells respectively overnight at 4℃. After rinsing with PBS for 3 times, the samples were incubated with Alexa Fluor 594 or 488 (1:500, Thermo Fisher Scientific) for 2 hours in darkness at room temperature. Nuclei were counterstained with DAPI (SouthernBiotech, 0100-20). Staining was visualized using confocal microscope (LSM800, Carl Zeiss, Oberkochen, Germany).

Lentivirus-mediated overexpression

Mouse Itga6 cDNA was amplified by PCR and cloned into the pLVX-FLEX-EF1a-ZsGreen lentiviral vector. The correct sequence of Itga6 gene in this construct was verified by sequencing. We cloned the expression cassette in an inverse, anti-sense orientation between two different loxP sites. The construct was designed so that Cre induction could be used to mediate the inversion of the Itga6 cassette into a sense orientation. Control or Itga6 lentivirus (10^9 TU per mouse) was injected into *Apoe*$^{-/-}$*/Tagln-Cre* or *Apoe*$^{-/-}$*/Hint1*^{SMKO} mice via tail vein, in which Cre induction mediated an initial flipping based on orientation and location of two loxP sites.

Chromatin immunoprecipitation

Chromatin immunoprecipitation was performed using a ChIP Assay Kit (Beyotime) according to manufacturer's protocol. Briefly, 1% formaldehyde was added to fix cells at 37 °C for 10 min, followed by neutralization using 125 mmol/L glycine. The cells were then washed with cold PBS and lysed on ice in SDS lysis buffer supplemented with proteinase inhibitor. The lysates were sonicated on ice. After centrifugation, the supernatant was collected and the chromatin in the supernatant was immunoprecipitated with anti-TFAP2A antibody (PA5-17359, invitrogen) or IgG (control) incubation at 4 °C overnight. Protein A/G beads were added and incubated for 2h at 4 °C. After reversing the cross-links, DNA was isolated and used for PCR reactions. Primers used for ChIP assay:

Itga6: Forward (5' to 3' sequence)：TTCCTTTACAGGGGTGGCTA

Reverse (5' to 3' sequence)：AGAGTCCCCGTGGTTCAGA

Statistical analysis

All values are presented in the figures as mean ± SEM with $P<0.05$ considered statistically significant. Fisher exact test was used for the incidence statistics of aortic aneurysm. For the comparison of the means between 2 groups, the Levene test was applied to evaluate the homogeneity of variance. An unpaired 2-sided Student t test was used when data showed equal variance; otherwise, t test assuming unequal variance was applied. For comparisons among more than 2 groups, Brown-Forsythe test was used to evaluate homogeneity of variance. If the data showed equal variance, a 1-way ANOVA analysis was used followed by a post hoc analysis using the Bonferroni method to adjust for multiple comparisons; otherwise, a Welch ANOVA test was performed followed by a post hoc analysis using the Tamhane T2 method. Two-way ANOVA followed by Tukey multiple comparisons test for post hoc comparisons was used when appropriate. Two-way ANOVA with mixed-effects was used for comparing the blood pressure of mice that were repeatedly measured over time, at 0 to 28 days after osmotic pumps implantation. Statistical results and the corresponding methods were presented in figure legends. All statistical analyses were performed and graphs were generated using GraphPad Prism 9.

Study approval

The use of human aortic tissue was approved by the medical ethics committee of Nanjing Drum Tower Hospital following the Declaration of Helsinki. Written informed consent was provided by all participants or the organ donors' legal representatives before enrollment. All animal experiments were conducted in accordance with the

ARRIVE guidelines for the care and use of laboratory animals, and with approval of the Nanjing Medical University Animal Care and Use Committee.

Data availability

Values for all data points in graphs are reported in the Supporting Data Values file.The RNA-Seq data reported in this study have been deposited in the Gene Expression Omnibus (GEO) database (GSE289426).

Author Contributions

Y.J., L.X., Y.H., and Y.Z. developed the concept, designed the study, and revised the manuscript. Y.Z. and W.W. analysed the data and drafted the manuscript. Y.Z., W.W., X.Y., S.L., X.W., Q.D., K.Y., L.H., and S.S. performed the experiments. X.D., Z.H. and X.L. provided clinical samples. Y.J., L.X., Y.H., F.C., A.G., L.W., Z.Z., B.Y. , C.Y. and Y.H. supervised the study. The order of co-first authors was determined by the volume of work each contributed to the study.

Acknowledgements

This work was supported by the National Natural Science Foundation of China (82121001), the National Key Research and Development Program of China (2019YFA0802704), grants from the National Natural Science Foundation of China (82241211, 82030013, 82222009, 82470496, 82370491), Natural Science Foundation of Jiangsu Province (BK20231260). The authors thank Dr. Jingjing Ben (Department of Pathophysiology, Nanjing Medical University, Nanjing, China) for sharing pLVX-FLEX-EF1a-ZsGreen plasmid.

References

1. Song T, et al. SLC44A2 regulates vascular smooth muscle cell phenotypic switching and aortic aneurysm. *J Clin Invest.* 2024;134(16):e173690.
2. Zhang Y, et al. S-Nitrosylation of Septin2 Exacerbates Aortic Aneurysm and Dissection by Coupling the TIAM1-RAC1 Axis in Macrophages. *Circulation.* 2024;149(24):1903-20.
3. Luo S, et al. Endothelial HDAC1-ZEB2-NuRD Complex Drives Aortic Aneurysm and Dissection Through Regulation of Protein S-Sulfhydration. *Circulation.* 2023;147(18):1382-403.
4. Zhao G, et al. BAF60c prevents abdominal aortic aneurysm formation through epigenetic control of vascular smooth muscle cell homeostasis. *J Clin Invest.* 2022;132(21):e158309.
5. Yap C, et al. Six Shades of Vascular Smooth Muscle Cells Illuminated by KLF4 (Kruppel-Like Factor 4). *Arterioscler Thromb Vasc Biol.* 2021;41(11):2693-707.
6. Luo Y, et al. The activator protein-1 complex governs a vascular degenerative transcriptional programme in smooth muscle cells to trigger aortic dissection and rupture. *Eur Heart J.* 2024;45(4):287-305.
7. Clement M, et al. Vascular Smooth Muscle Cell Plasticity and Autophagy in Dissecting Aortic Aneurysms. *Arterioscler Thromb Vasc Biol.* 2019;39(6):1149-59.
8. Zhou C, et al. Anxa1 in smooth muscle cells protects against acute aortic dissection. *Cardiovasc Res.* 2022;118(6):1564-82.

9. Davis-Dusenbery BN, et al. Micromanaging vascular smooth muscle cell differentiation and phenotypic modulation. *Arterioscler Thromb Vasc Biol.* 2011;31(11):2370-7.

10. Cordes KR, et al. miR-145 and miR-143 regulate smooth muscle cell fate and plasticity. *Nature.* 2009;460(7256):705-10.

11. Liu R, et al. ARHGAP18 Protects Against Thoracic Aortic Aneurysm Formation by Mitigating the Synthetic and Proinflammatory Smooth Muscle Cell Phenotype. *Circ Res.* 2017;121(5):512-24.

12. Bunton TE, et al. Phenotypic alteration of vascular smooth muscle cells precedes elastolysis in a mouse model of Marfan syndrome. *Circ Res.* 2001;88(1):37-43.

13. Brenner C, et al. Crystal structures of HINT demonstrate that histidine triad proteins are GalT-related nucleotide-binding proteins. *Nat Struct Biol.* 1997;4(3):231-8.

14. Morel V, et al. HINT1 neuropathy: Expanding the genotype and phenotype spectrum. *Clin Genet.* 2022;102(5):379-90.

15. Liu P, et al. HINT1 in Neuropsychiatric Diseases: A Potential Neuroplastic Mediator. *Neural Plast.* 2017;2017:5181925.

16. Wang L, et al. Hint1 inhibits growth and activator protein-1 activity in human colon cancer cells. *Cancer Res.* 2007;67(10):4700-8.

17. Li H, et al. The HINT1 tumor suppressor regulates both gamma-H2AX and ATM in response to DNA damage. *J Cell Biol.* 2008;183(2):253-65.

724 18. Motzik A, et al. Post-translational modification of HINT1 mediates activation
725 of MITF transcriptional activity in human melanoma cells. *Oncogene.*
726 2017;36(33):4732-8.
727 19. Wang L, et al. HINT1 inhibits beta-catenin/TCF4, USF2 and NFkappaB activity
728 in human hepatoma cells. *Int J Cancer.* 2009;124(7):1526-34.
729 20. Zhang Y, et al. HINT1 (Histidine Triad Nucleotide-Binding Protein 1)
730 Attenuates Cardiac Hypertrophy Via Suppressing HOXA5 (Homeobox A5)
731 Expression. *Circulation.* 2021;144(8):638-54.
732 21. Munshaw S, et al. Thymosin β4 protects against aortic aneurysm via endocytic
733 regulation of growth factor signaling. *J Clin Invest.* 2021;131(10):e127884.
734 22. Lei C, et al. FAM3A reshapes VSMC fate specification in abdominal aortic
735 aneurysm by regulating KLF4 ubiquitination. *Nat Commun.* 2023;14(1):5360.
736 23. Shi D, et al. TFAP2A regulates nasopharyngeal carcinoma growth and survival
737 by targeting HIF-1alpha signaling pathway. *Cancer Prev Res (Phila).*
738 2014;7(2):266-77.
739 24. Radu A, et al. The peptide repeat domain of nucleoporin Nup98 functions as a
740 docking site in transport across the nuclear pore complex. *Cell.* 1995;81(2):215-
741 22.
742 25. Iwamoto M, et al. Nucleoporin Nup98: a gatekeeper in the eukaryotic kingdoms.
743 *Genes Cells.* 2010;15(7):661-9.
744 26. Herrmann A, et al. Integrin alpha6 signaling induces STAT3-TET3-mediated
745 hydroxymethylation of genes critical for maintenance of glioma stem cells.

Oncogene. 2020;39(10):2156-69.

27. Gao X, et al. Physiological stretch induced proliferation of human urothelial cells via integrin alpha6-FAK signaling pathway. *Neurourol Urodyn.* 2018;37(7):2114-20.

28. Sayers RL, et al. FRNK expression promotes smooth muscle cell maturation during vascular development and after vascular injury. *Arterioscler Thromb Vasc Biol.* 2008;28(12):2115-22.

29. Dawson JC, et al. Targeting FAK in anticancer combination therapies. *Nat Rev Cancer.* 2021;21(5):313-24.

30. Jia Y, et al. PHB2 Maintains the Contractile Phenotype of VSMCs by Counteracting PKM2 Splicing. *Circ Res.* 2022;131(10):807-24.

31. Miano JM, et al. Fate and State of Vascular Smooth Muscle Cells in Atherosclerosis. *Circulation.* 2021;143(21):2110-6.

32. Zhao G, et al. Unspliced XBP1 Confers VSMC Homeostasis and Prevents Aortic Aneurysm Formation via FoxO4 Interaction. *Circ Res.* 2017;121(12):1331-45.

33. Yao H, et al. Leukaemia hijacks a neural mechanism to invade the central nervous system. *Nature.* 2018;560(7716):55-60.

34. Chen WC, et al. BMP-2 induces angiogenesis by provoking integrin alpha6 expression in human endothelial progenitor cells. *Biochem Pharmacol.* 2018;150:256-66.

35. Groulx JF, et al. Integrin alpha6A splice variant regulates proliferation and the

768 Wnt/beta-catenin pathway in human colorectal cancer cells. *Carcinogenesis.*
769 2014;35(6):1217-27.
770 36. Sulzmaier FJ, et al. FAK in cancer: mechanistic findings and clinical
771 applications. *Nat Rev Cancer.* 2014;14(9):598-610.
772 37. Lee BY, et al. FAK signaling in human cancer as a target for therapeutics.
773 *Pharmacol Ther.* 2015;146:132-49.
774 38. Ilic D, et al. Reduced cell motility and enhanced focal adhesion contact
775 formation in cells from FAK-deficient mice. *Nature.* 1995;377(6549):539-44.
776 39. Ilic D, et al. Focal adhesion kinase is required for blood vessel morphogenesis.
777 *Circ Res.* 2003;92(3):300-7.
778 40. Cheng Z, et al. Focal adhesion kinase regulates smooth muscle cell recruitment
779 to the developing vasculature. *Arterioscler Thromb Vasc Biol.*
780 2011;31(10):2193-202.
781 41. Le Coq J, et al. New insights into FAK structure and function in focal adhesions.
782 *J Cell Sci.* 2022;135(20):jcs259089.
783 42. Jeong K, et al. FAK Activation Promotes SMC Dedifferentiation via Increased
784 DNA Methylation in Contractile Genes. *Circ Res.* 2021;129(12):e215-e33.
785 43. Wang-Gillam A, et al. Defactinib, Pembrolizumab, and Gemcitabine in Patients
786 with Advanced Treatment Refractory Pancreatic Cancer: A Phase I Dose
787 Escalation and Expansion Study. *Clin Cancer Res.* 2022;28(24):5254-62.
788 44. Bossone E, et al. Epidemiology and management of aortic disease: aortic
789 aneurysms and acute aortic syndromes. *Nat Rev Cardiol.* 2021;18(5):331-48.

45. Sawada H, et al. Twenty Years of Studying AngII (Angiotensin II)-Induced Abdominal Aortic Pathologies in Mice: Continuing Questions and Challenges to Provide Insight Into the Human Disease. *Arterioscler Thromb Vasc Biol.* 2022;42(3):277-88.

46. Chen HZ, et al. Age-Associated Sirtuin 1 Reduction in Vascular Smooth Muscle Links Vascular Senescence and Inflammation to Abdominal Aortic Aneurysm. *Circ Res.* 2016;119(10):1076-88.

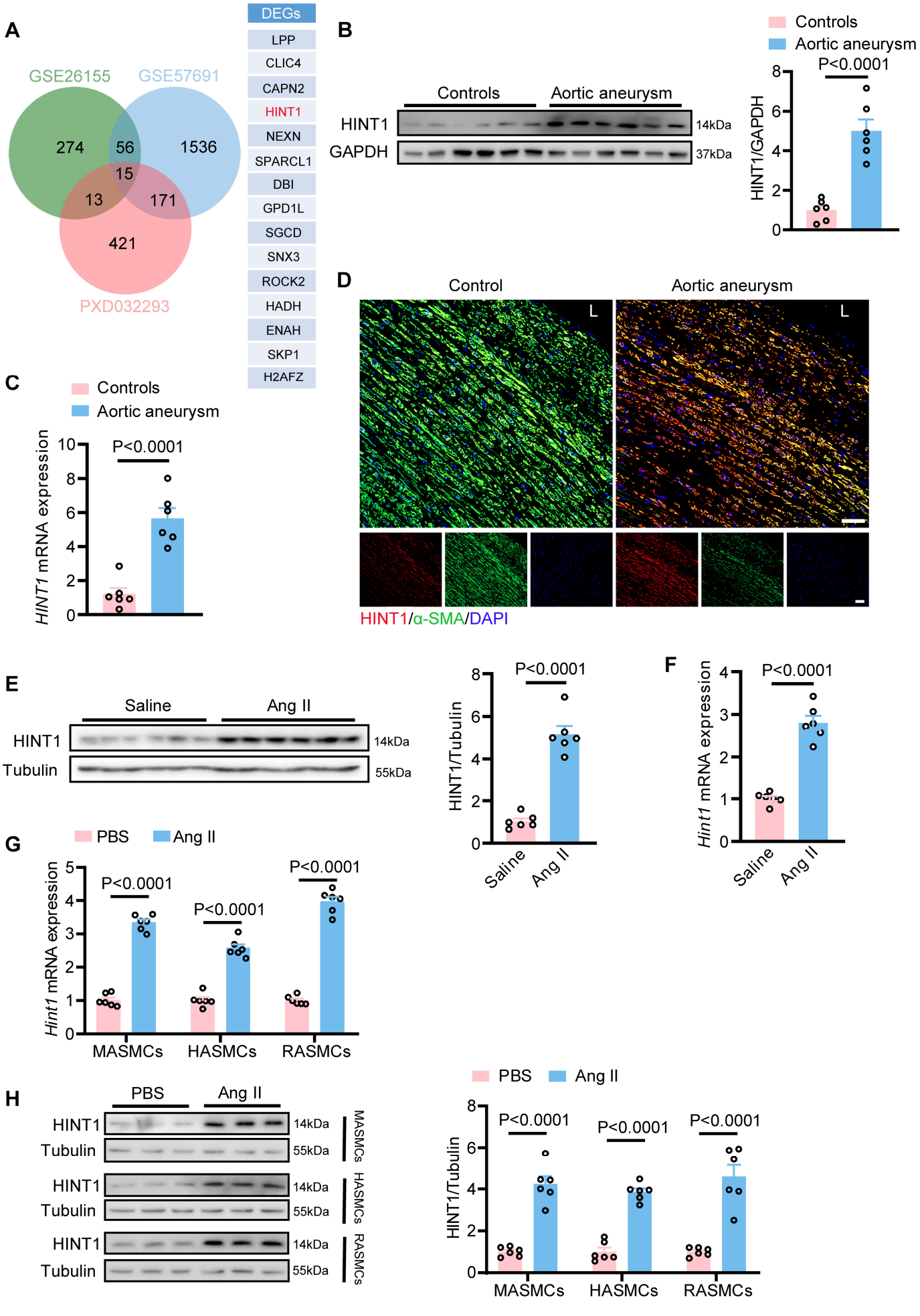
A
GSE26155
GSE57691
PXD032293
274
56
1536
15
13
171
421
DEGs
LPP
CLIC4
CAPN2
HINT1
NEXN
SPARCL1
DBI
GPD1L
SGCD
SNX3
ROCK2
HADH
ENAH
SKP1
H2AFZ
B
Controls
Aortic aneurysm
HINT1
GAPDH
14kDa
37kDa
HINT1/GAPDH
P<0.0001
C
Controls
Aortic aneurysm
HINT1 mRNA expression
P<0.0001
D
Control
Aortic aneurysm
L
HINT1/α-SMA/DAPI
E
Saline
Ang II
HINT1
Tubulin
14kDa
55kDa
HINT1/Tubulin
P<0.0001
F
Hint1 mRNA expression
P<0.0001
G
PBS
Ang II
Hint1 mRNA expression
P<0.0001
P<0.0001
P<0.0001
MASMCs
HASMCs
RASMCs
H
PBS
Ang II
HINT1
Tubulin
14kDa
55kDa
MASMCs
HASMCs
RASMCs
HINT1/Tubulin
P<0.0001
P<0.0001
P<0.0001

Figure 1: Upregulation of HINT1 correlates with aortic aneurysm.

(**A**), Differentially expressed genes/proteins were identified from aortic tissue of aortic aneurysm patients than controls in three databases (Green-GSE57691, Blue-GSE26155 and Red-PXD03229). Venn diagram showing the comparison among the three datasets identified 15 overlapping targets. (**B and C**), Western blotting (**B**) and qPCR (**C**) analysis of HINT1 expression in aorta samples from aortic aneurysm patients and normal aorta samples from donors. n=6 per group. (**D**), Representative immunofluorescence images of α-SMA and HINT1 in aortic samples from aortic aneurysm patients and non-aortic aneurysm controls; red: HINT1; green: α-SMA; blue: DAPI; L: Lumen; scale bar= 50 μm. (**E and F**), Eight-week-old male *Apoe*$^{-/-}$ mice were infused with saline or Angiotensin II (Ang II; 1000 ng/kg/min) for 28 days. Western blotting (**E**) and qPCR (**F**) analysis of HINT1 expression in mouse suprarenal abdominal aortas. n=6 per group. (**G**), Mouse aortic smooth muscle cells (MASMCs) were isolated from the whole aortas of mice. qPCR analysis of the mRNA levels of *Hint1* in isolated mouse aortic smooth muscle cells (MASMCs), human aortic smooth muscle cells (HASMCs) and rat aortic smooth muscle cells (RASMCs) stimulated with PBS or Ang II (10^{-6} M). n=6 per group. (**H**), MASMCs were isolated from the whole aortas of mice. Western blotting analysis of HINT1 in MASMCs, HASMCs and RASMCs stimulated with PBS or Ang II (10^{-6} M). n=6 per group. Statistical analysis was performed by Student *t* test for (**B**, **C**, **E** through **H**). For all statistical plots, the data are presented as mean ± SEM.

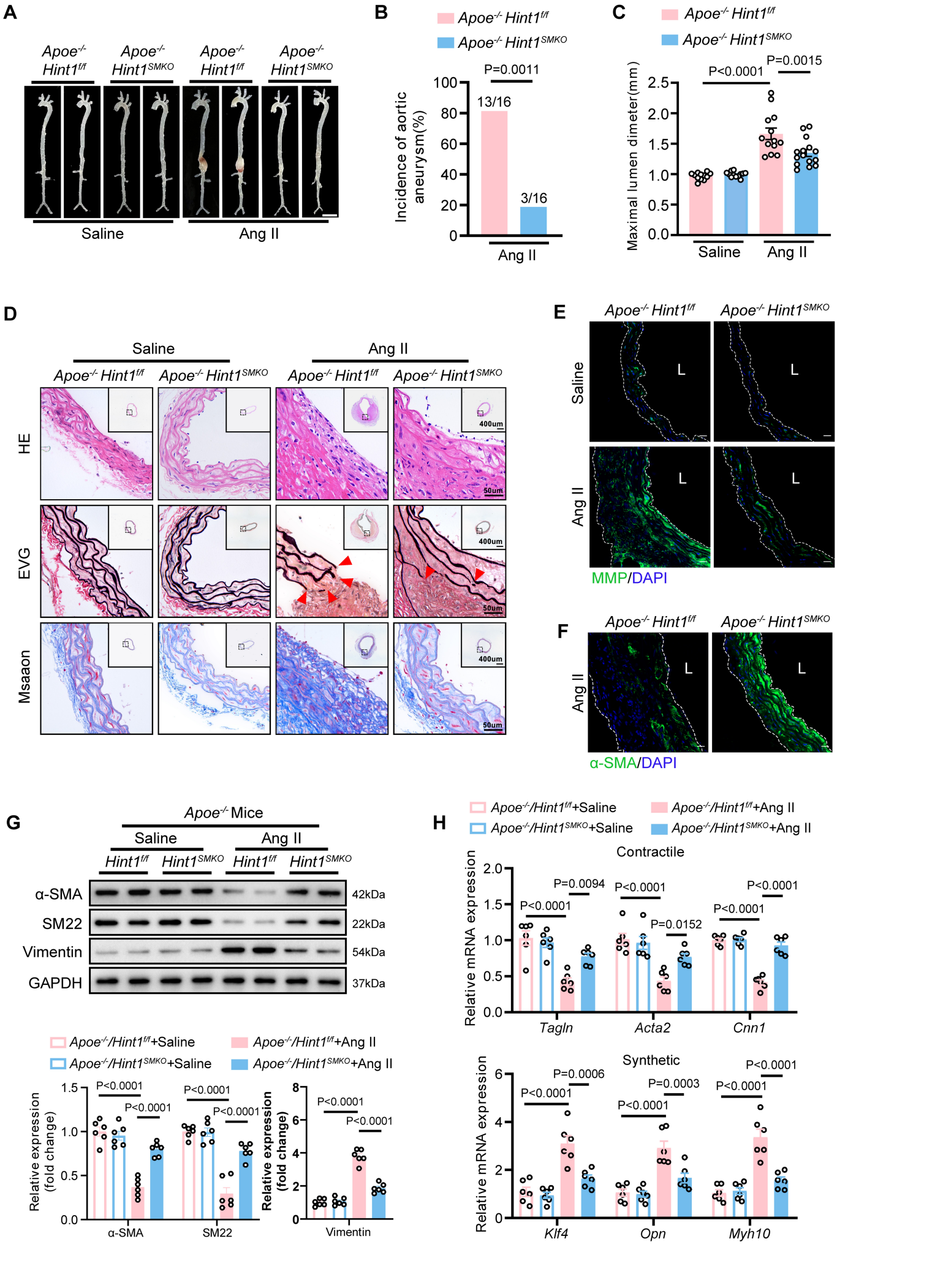
A
Apoe-/- Hint1f/f
Apoe-/- Hint1SMKO
Apoe-/- Hint1f/f
Apoe-/- Hint1SMKO
Saline
Ang II
B
Apoe-/- Hint1f/f
Apoe-/- Hint1SMKO
P=0.0011
13/16
3/16
Incidence of aortic aneurysm(%)
Ang II
C
Apoe-/- Hint1f/f
Apoe-/- Hint1SMKO
P<0.0001
P=0.0015
Maximal lumen dimeter(mm)
Saline
Ang II
D
Saline
Ang II
Apoe-/- Hint1f/f
Apoe-/- Hint1SMKO
Apoe-/- Hint1f/f
Apoe-/- Hint1SMKO
HE
EVG
Msaaon
400um
50um
E
Apoe-/- Hint1f/f
Apoe-/- Hint1SMKO
Saline
Ang II
L
MMP/DAPI
F
Apoe-/- Hint1f/f
Apoe-/- Hint1SMKO
Ang II
L
α-SMA/DAPI
G
Apoe-/- Mice
Saline
Ang II
Hint1f/f
Hint1SMKO
Hint1f/f
Hint1SMKO
α-SMA
SM22
Vimentin
GAPDH
42kDa
22kDa
54kDa
37kDa
Apoe-/-/Hint1f/f+Saline
Apoe-/-/Hint1f/f+Ang II
Apoe-/-/Hint1SMKO+Saline
Apoe-/-/Hint1SMKO+Ang II
Relative expression (fold change)
P<0.0001
P<0.0001
P<0.0001
P<0.0001
P<0.0001
P<0.0001
α-SMA
SM22
Vimentin
H
Apoe-/-/Hint1f/f+Saline
Apoe-/-/Hint1f/f+Ang II
Apoe-/-/Hint1SMKO+Saline
Apoe-/-/Hint1SMKO+Ang II
Contractile
Relative mRNA expression
P<0.0001
P=0.0094
P<0.0001
P=0.0152
P<0.0001
P<0.0001
Tagln
Acta2
Cnn1
Synthetic
Relative mRNA expression
P<0.0001
P=0.0006
P<0.0001
P=0.0003
P<0.0001
P<0.0001
Klf4
Opn
Myh10

Figure 2: *Hint1* deficiency in vascular smooth muscle cells mitigates aortic aneurysm.

Saline (n=12 per group) or Ang II (1000 ng/kg/min) (n=16 per group) was infused subcutaneously in *Apoe*$^{-/-}$*/Hint1*$^{flox/flox}$ (*Apoe*$^{-/-}$*/Hint1*$^{f/f}$) and *Apoe*$^{-/-}$*/Hint1*^{SMKO} mice for 28 days. (**A**), Representative photograph of aortas from *Apoe*$^{-/-}$*/Hint1*$^{f/f}$ and *Apoe*$^{-/-}$*/Hint1*^{SMKO} mice after saline or Ang II infusion. (**B**), Incidence of Ang II-induced aortic aneurysm. (**C**), Maximal abdominal lumen diameter of saline (n=12) or Ang II (n=13-16) infused mice measured by ultrasound. (**D**), Histopathological images of suprarenal abdominal aortas of *Apoe*$^{-/-}$*/Hint1*$^{f/f}$ and *Apoe*$^{-/-}$*/Hint1*^{SMKO} mice after 28 days of saline or Ang II infusion; scale bar = 50 and 400 μm. HE, hematoxylin-eosin staining; EVG, Elastic Van Gieson staining. (**E**), Representative in situ zymography photomicrographs showing matrix metalloproteinase (MMP) activity of suprarenal abdominal aortas; scale bar = 20 μm; L: Lumen; (**F**), Representative immunofluorescence staining of α-SMA expression in suprarenal abdominal aortas; scale bar = 20 μm; L: Lumen. (**G**), Western blotting analysis of the VSMC contractile markers (α-SMA and SM22) and synthetic markers (Vimentin) in suprarenal abdominal aortas from saline or Ang II-infused *Apoe*$^{-/-}$*/Hint1*$^{f/f}$ and *Apoe*$^{-/-}$*/Hint1*^{SMKO} mice. n=6 per group. (**H**), qPCR analysis of the mRNA levels of VSMC contractile markers (*Acta2, Tagln and Cnn1*) and synthetic markers (*Klf4, Opn, Myh10*) in suprarenal abdominal aortas from saline or Ang II-infused *Apoe*$^{-/-}$*/Hint1*$^{f/f}$ and *Apoe*$^{-/-}$*/Hint1*^{SMKO} mice. n=6 per group. Statistical analysis was performed by a Fisher exact test for (**B**), One-way ANOVA for (**C, G and H**). For all statistical plots, the data are presented as mean ± SEM.

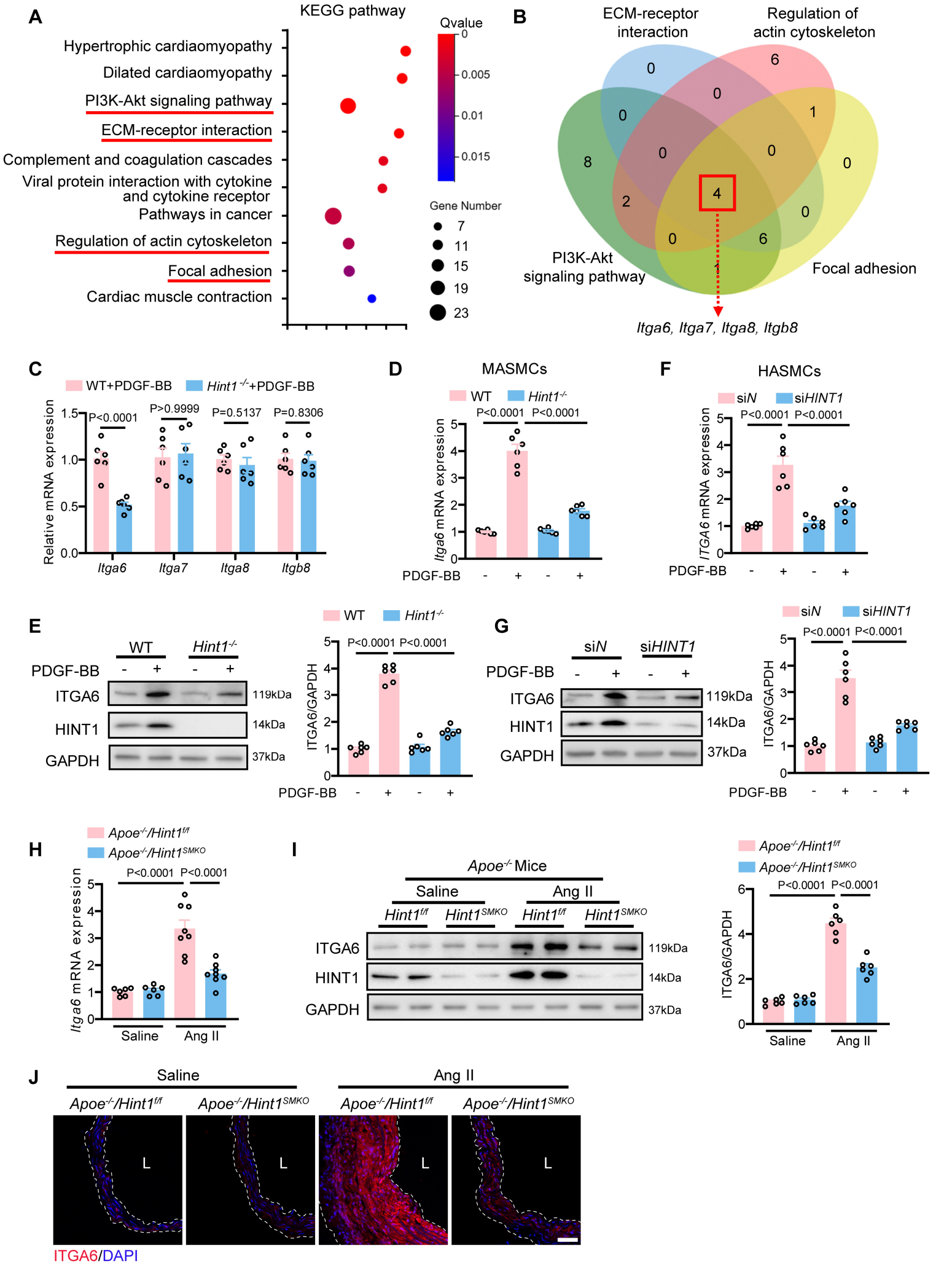
A
KEGG pathway
Hypertrophic cardiaomyopathy
Dilated cardiaomyopathy
PI3K-Akt signaling pathway
ECM-receptor interaction
Complement and coagulation cascades
Viral protein interaction with cytokine and cytokine receptor
Pathways in cancer
Regulation of actin cytoskeleton
Focal adhesion
Cardiac muscle contraction
Qvalue
0
0.005
0.01
0.015
Gene Number
7
11
15
19
23
B
ECM-receptor interaction
Regulation of actin cytoskeleton
PI3K-Akt signaling pathway
Focal adhesion
0
6
0
0
1
8
0
0
0
2
4
0
0
6
Itga6, Itga7, Itga8, Itgb8
C
WT+PDGF-BB
Hint1 -/-+PDGF-BB
Relative mRNA expression
P<0.0001
P>0.9999
P=0.5137
P=0.8306
Itga6
Itga7
Itga8
Itgb8
D
MASMCs
WT
Hint1-/-
Itga6 mRNA expression
P<0.0001
P<0.0001
PDGF-BB
F
HASMCs
siN
siHINT1
ITGA6 mRNA expression
P<0.0001
P<0.0001
PDGF-BB
E
WT
Hint1-/-
PDGF-BB
ITGA6
HINT1
GAPDH
119kDa
14kDa
37kDa
ITGA6/GAPDH
P<0.0001
P<0.0001
G
siN
siHINT1
PDGF-BB
ITGA6
HINT1
GAPDH
119kDa
14kDa
37kDa
ITGA6/GAPDH
P<0.0001
P<0.0001
H
Apoe-/-Hint1f/f
Apoe-/-Hint1SMKO
Itga6 mRNA expression
P<0.0001
P<0.0001
Saline
Ang II
I
Apoe-/- Mice
Saline
Ang II
Hint1f/f
Hint1SMKO
Hint1f/f
Hint1SMKO
ITGA6
HINT1
GAPDH
119kDa
14kDa
37kDa
Apoe-/-Hint1f/f
Apoe-/-Hint1SMKO
ITGA6/GAPDH
P<0.0001
P<0.0001
Saline
Ang II
J
Saline
Ang II
Apoe-/-Hint1f/f
Apoe-/-Hint1SMKO
Apoe-/-Hint1f/f
Apoe-/-Hint1SMKO
L
L
L
L
ITGA6/DAPI

Figure 3: ITGA6 is the downstream target of HINT1.

(**A**), Kyoto Encyclopedia of Genes and Genomes (KEGG) pathway analysis of differential expression genes in PDGF-BB-treated MASMCs isolated from the whole aorta of WT and *Hint1*$^{-/-}$ mice. (**B**), Venn diagram showing 4 overlapping targets which were all enriched in the related pathways (ECM-receptor interaction (blue), Regulation of actin cytoskeleton (red), PI3K-Akt signaling pathway (green) and Focal adhesion (yellow)) in (**A**)**.** (**C**), qPCR analysis of above 4 overlapping targets (*Itga6*, *Itga7*, *Itga8*, *Itgb8*) in MASMCs isolated from the whole aorta of WT and *Hint1*$^{-/-}$ mice and treated with PDGF-BB (20 ng/ml). n=6 per group. (**D and E**), qPCR (**D**) and Western blotting (**E**) analysis of *Itga6* in MASMCs isolated from the whole aorta of WT and *Hint1*$^{-/-}$ mice and treated with PBS or PDGF-BB (20 ng/ml). n=6 per group. (**F and G**), qPCR (**F**) and Western blotting (**G**) analysis of *Itga6* in HASMCs that transfected with si*N* or si*HINT1* followed by PBS or PDGF-BB (20 ng/ml) stimulation. n=6 per group. (**H through J**), Eight-week-old male *Apoe*$^{-/-}$*/Hint1*$^{f/f}$ and *Apoe*$^{-/-}$*/Hint1*^{SMKO} mice were infused with saline or Ang II (1000 ng/kg/min) for 28 days. qPCR (**H**) and Western blotting (**I**) analysis of the levels of *Itga6* in aortas. n=6-8 per group. (**J**), Representative immunofluorescence staining of ITGA6 expression in abdominal aortas; scale bar = 20 μm; L: Lumen. Statistical analysis was performed by Student *t* test for (**C**), One-way ANOVA for (**D through I**). For all statistical plots, the data are presented as mean ± SEM.

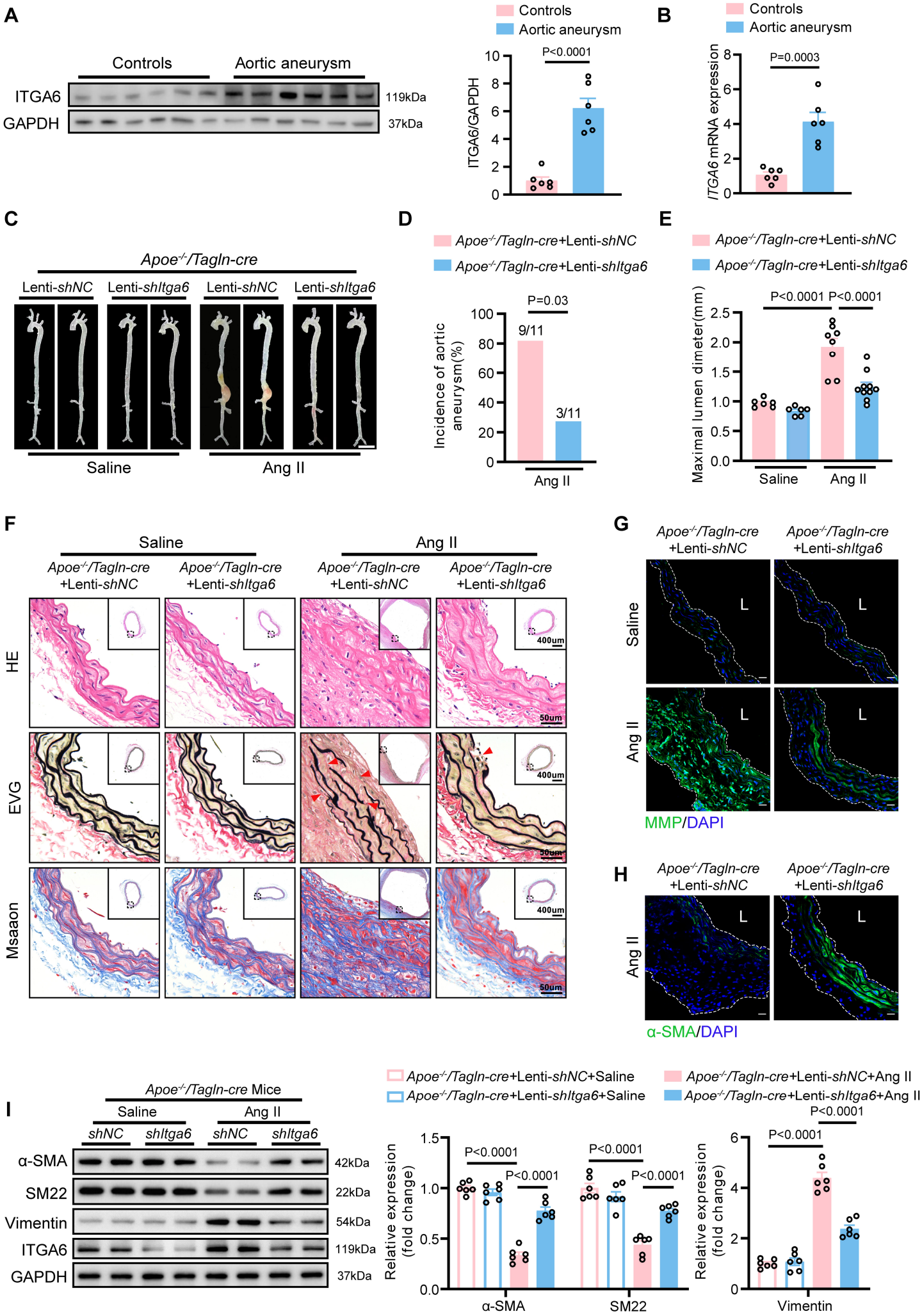
A
Controls
Aortic aneurysm
ITGA6
GAPDH
119kDa
37kDa
Controls
Aortic aneurysm
P<0.0001
ITGA6/GAPDH
B
Controls
Aortic aneurysm
P=0.0003
ITGA6 mRNA expression
C
Apoe-/-/Tagln-cre
Lenti-shNC
Lenti-shItga6
Lenti-shNC
Lenti-shItga6
Saline
Ang II
D
Apoe-/-/Tagln-cre+Lenti-shNC
Apoe-/-/Tagln-cre+Lenti-shItga6
P=0.03
9/11
3/11
Incidence of aortic aneurysm(%)
Ang II
E
Apoe-/-/Tagln-cre+Lenti-shNC
Apoe-/-/Tagln-cre+Lenti-shItga6
P<0.0001
P<0.0001
Maximal lumen dimeter(mm)
Saline
Ang II
F
Saline
Ang II
Apoe-/-/Tagln-cre +Lenti-shNC
Apoe-/-/Tagln-cre +Lenti-shItga6
HE
EVG
Msaaon
400um
50um
G
Apoe-/-/Tagln-cre +Lenti-shNC
Apoe-/-/Tagln-cre +Lenti-shItga6
Saline
Ang II
L
MMP/DAPI
H
Apoe-/-/Tagln-cre +Lenti-shNC
Apoe-/-/Tagln-cre +Lenti-shItga6
Ang II
L
α-SMA/DAPI
I
Apoe-/-/Tagln-cre Mice
Saline
Ang II
shNC
shItga6
shNC
shItga6
α-SMA
SM22
Vimentin
ITGA6
GAPDH
42kDa
22kDa
54kDa
119kDa
37kDa
Apoe-/-/Tagln-cre+Lenti-shNC+Saline
Apoe-/-/Tagln-cre+Lenti-shItga6+Saline
Apoe-/-/Tagln-cre+Lenti-shNC+Ang II
Apoe-/-/Tagln-cre+Lenti-shItga6+Ang II
Relative expression (fold change)
P<0.0001
P<0.0001
P<0.0001
P<0.0001
α-SMA
SM22
P<0.0001
P<0.0001
Vimentin

Figure 4: Knockdown of *Itga6* in vascular smooth muscle cells mitigates aortic aneurysm.

(**A and B**), Western blotting (**A**) and qPCR (**B**) analysis of ITGA6 in aorta samples from aortic aneurysm patients and normal aorta samples from donors. n=6 per group. Six-week-old male *Apoe*$^{-/-}$*/Tagln-cre* mice were injected with lentivirus vector encoding negative shRNA control (Lenti-sh*NC*) or lentivirus vector encoding shRNA targeting Itga6 (Lenti-*shItga6*) with 2 reverse loxP sites, which can be recognized by Cre recombinase. After infection for 14 days, mice were infused with saline or angiotensin II (Ang II; 1000 ng/kg/min) for 28 days. (**C**), Representative photograph of aortas from saline or Ang II-infused *Apoe*$^{-/-}$*/Tagln-cre* mice infected with Lenti-sh*NC* or Lenti-sh*Itga6*. (**D**), Incidence of Ang II-induced aortic aneurysm. (**E**), Maximal abdominal lumen diameter of saline (n=6) or Ang II (n=8-10) infused mice measured by ultrasound. (**F**), Histopathological images of suprarenal abdominal aortas of saline or Ang II-infused *Apoe*$^{-/-}$*/Tagln-cre* mice infected with Lenti-sh*NC* or Lenti-sh*Itga6*. scale bar = 50 and 400 μm. (**G**), Representative in situ zymography photomicrographs showing matrix metalloproteinase (MMP) activity of suprarenal abdominal aortas; scale bar = 20 μm; L: Lumen. (**H**), Representative immunofluorescence staining of α-SMA expression in suprarenal abdominal aortas; scale bar = 20 μm; L: Lumen. (**I**), Western blotting analysis of the VSMCs contractile markers (α-SMA and SM22) and synthetic markers (Vimentin) in suprarenal abdominal aortas from saline or Ang II-infused *Apoe*$^{-/-}$*/Tagln-cre* mice infected with Lenti-sh*NC* or Lenti-sh*Itga6*. n=6 per group. Statistical analysis was performed by Student *t* test for (**A and B**), a Fisher exact test for (**D**), One-way ANOVA for (**E and I**). For all statistical plots, the data are presented as mean ± SEM.

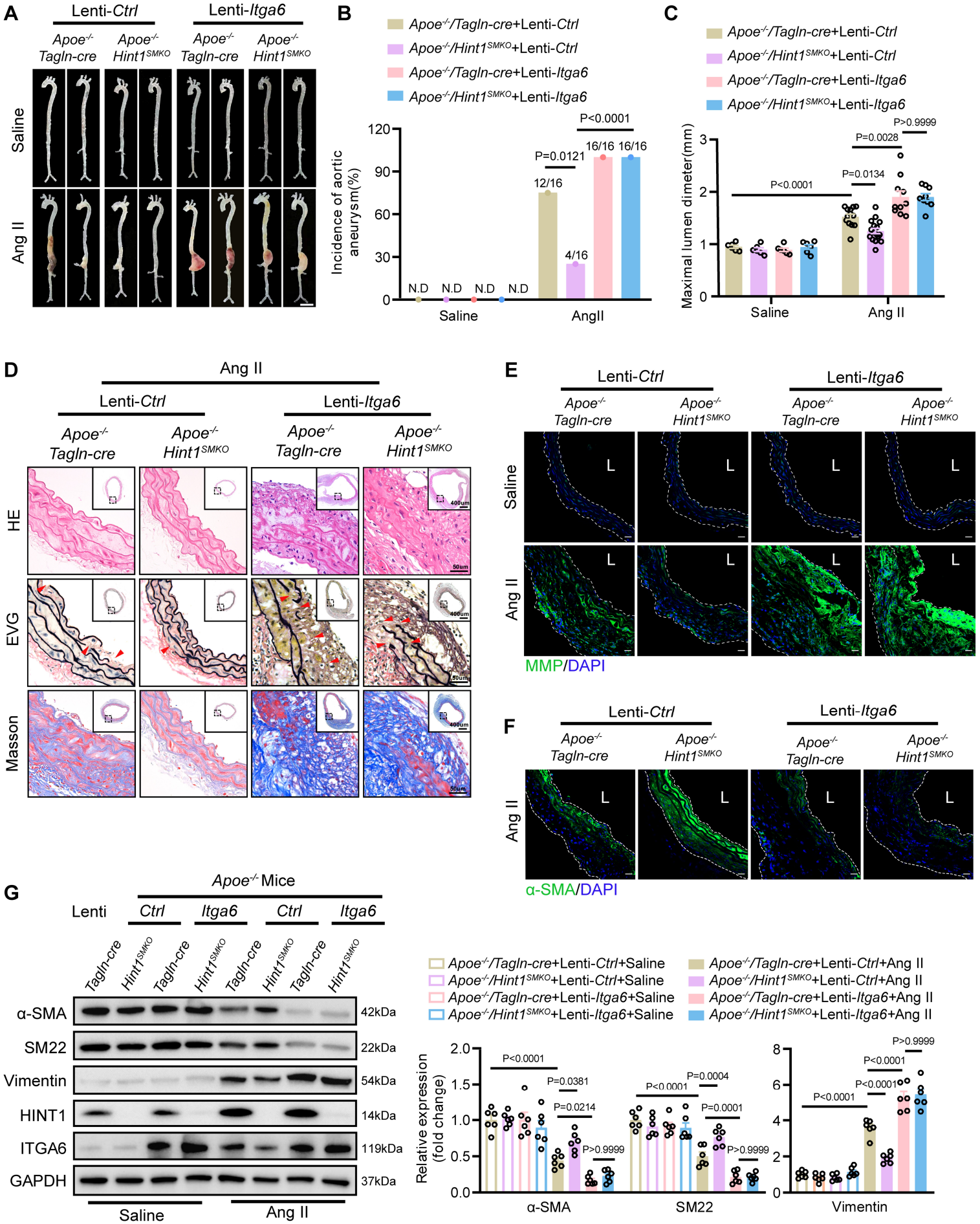
A
Lenti-Ctrl
Lenti-Itga6
Apoe-/- Tagln-cre
Apoe-/- Hint1SMKO
Saline
Ang II
B
Apoe-/-/Tagln-cre+Lenti-Ctrl
Apoe-/-/Hint1SMKO+Lenti-Ctrl
Apoe-/-/Tagln-cre+Lenti-Itga6
Apoe-/-/Hint1SMKO+Lenti-Itga6
Incidence of aortic aneurysm(%)
P<0.0001
P=0.0121
16/16
16/16
12/16
4/16
N.D
Saline
AngII
C
Maximal lumen dimeter(mm)
P>0.9999
P=0.0028
P=0.0134
P<0.0001
Saline
Ang II
D
Ang II
HE
EVG
Masson
E
MMP/DAPI
F
α-SMA/DAPI
G
Apoe-/- Mice
Lenti
Ctrl
Itga6
α-SMA
SM22
Vimentin
HINT1
ITGA6
GAPDH
42kDa
22kDa
54kDa
14kDa
119kDa
37kDa
Apoe-/-/Tagln-cre+Lenti-Ctrl+Saline
Apoe-/-/Hint1SMKO+Lenti-Ctrl+Saline
Apoe-/-/Tagln-cre+Lenti-Itga6+Saline
Apoe-/-/Hint1SMKO+Lenti-Itga6+Saline
Apoe-/-/Tagln-cre+Lenti-Ctrl+Ang II
Apoe-/-/Hint1SMKO+Lenti-Ctrl+Ang II
Apoe-/-/Tagln-cre+Lenti-Itga6+Ang II
Apoe-/-/Hint1SMKO+Lenti-Itga6+Ang II
Relative expression (fold change)
P<0.0001
P=0.0381
P=0.0214
P>0.9999
P=0.0004
P=0.0001
P<0.0001
P<0.0001
P<0.0001
P>0.9999

Figure 5: Impact of HINT1 on aortic aneurysm relies on its regulation of ITGA6 *in vivo*.

Six-week-old male *Apoe*$^{-/-}$*/Tagln-cre* and *Apoe*$^{-/-}$*/Hint1*^{SMKO} mice were injected with lentivirus vectors encoding control (Lenti-*Ctrl*) or *Itga6* (Lenti-*Itga6*) with 2 reverse loxP sites, which can be recognized by Cre recombinase. After infection for 14 days, mice were infused with saline or angiotensin II (Ang II; 1000 ng/kg/min) for 28 days. (**A**), Representative photograph of aortas from saline or Ang II-infused *Apoe*$^{-/-}$*/Tagln-cre* or *Apoe*$^{-/-}$*/Hint1*^{SMKO} mice infected with Lenti-*Ctrl* or Lenti-*Itga6*. (**B**), Incidence of Ang II-induced aortic aneurysm. (**C**), Maximal abdominal lumen diameter of saline (n=6) or Ang II (n=9-16) infused mice measured by ultrasound. (**D**), Histopathological images of suprarenal abdominal aortas of saline or Ang II-infused *Apoe*$^{-/-}$*/Tagln-cre* or *Apoe*$^{-/-}$*/Hint1*^{SMKO} mice infected with Lenti-*Ctrl* or Lenti-*Itga6*; scale bar = 50 and 400 μm. (**E**), Representative in situ zymography photomicrographs showing matrix metalloproteinase (MMP) activity of suprarenal abdominal aortas; scale bar = 20 μm; L: Lumen. (**F**), Representative immunofluorescence staining of α-SMA expression in suprarenal abdominal aortas; scale bar = 20 μm; L: Lumen. (**G**), Western blotting analysis of the VSMC contractile markers (α-SMA and SM22) and synthetic markers (Vimentin) in suprarenal abdominal aortas from saline or Ang II-infused *Apoe*$^{-/-}$*/Tagln-cre* or *Apoe*$^{-/-}$*/Hint1*^{SMKO} mice infected with Lenti-*Ctrl* or Lenti-*Itga6*. n=6 per group. Statistical analysis was performed by a Fisher exact test for (**B**), Two-way ANOVA for (**C and G**). For all statistical plots, the data are presented as mean ± SEM.

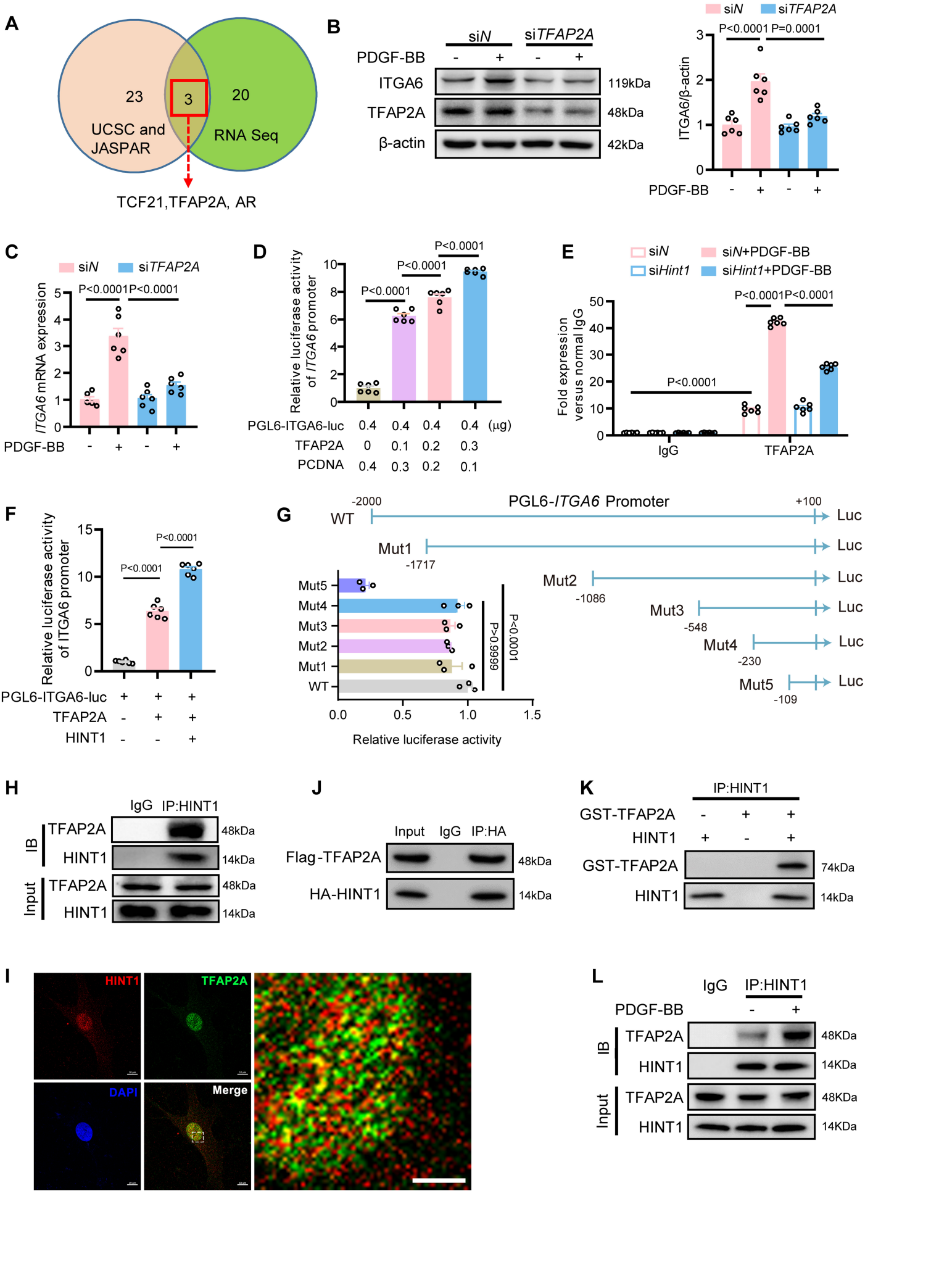
A
23
3
20
UCSC and JASPAR
RNA Seq
TCF21,TFAP2A, AR
B
siN
siTFAP2A
PDGF-BB
ITGA6
TFAP2A
β-actin
119kDa
48kDa
42kDa
ITGA6/β-actin
P<0.0001 P=0.0001
C
ITGA6 mRNA expression
P<0.0001P<0.0001
D
Relative luciferase activity of ITGA6 promoter
P<0.0001
PGL6-ITGA6-luc 0.4 0.4 0.4 0.4 (μg)
TFAP2A 0 0.1 0.2 0.3
PCDNA 0.4 0.3 0.2 0.1
E
siN
siN+PDGF-BB
siHint1
siHint1+PDGF-BB
Fold expression versus normal IgG
P<0.0001P<0.0001
IgG
TFAP2A
F
Relative luciferase activity of ITGA6 promoter
PGL6-ITGA6-luc
TFAP2A
HINT1
G
PGL6-ITGA6 Promoter
-2000
+100
WT
Mut1
-1717
Mut2
-1086
Mut3
-548
Mut4
-230
Mut5
-109
Luc
P<0.0001
P>0.9999
Relative luciferase activity
H
IgG IP:HINT1
IB
Input
TFAP2A
HINT1
48kDa
14kDa
J
Input IgG IP:HA
Flag-TFAP2A
HA-HINT1
K
IP:HINT1
GST-TFAP2A
HINT1
74kDa
I
HINT1
TFAP2A
DAPI
Merge
L
IgG IP:HINT1
PDGF-BB

Figure 6: HINT1 regulates ITGA6 expression via its interaction with TFAP2A.

(**A**), Venn diagram showing the potential transcription factors for ITGA6 which were regulated by HINT1. **Pink**, transcription factors for ITGA6 predicted by UCSC and JASPAR library. **Green**, differentially expressed transcription factors in PDGF-BB-treated WT and *Hint1*$^{-/-}$ MASMCs detected by RNA-Seq mentioned in **Figure 3A**. (**B and C**), Western blotting (**B**) and qPCR (**C**) analysis of ITGA6 expression in HASMCs that were transfected with si*N* or si*TFAP2A* followed by PBS or PDGF-BB stimulation. n=6. (**D**), Luciferase reporter constructs with full-length *Itga6* promoter were co-transfected with TFAP2A plasmid or PCDNA into HEK293T cells, and luciferase activity was evaluated. n=6. (**E**), Chromatin immunoprecipitation assays of TFAP2A binding to the ITGA6 promoter in RASMCs transfected with si*N* or si*Hint1* and treated with PBS or PDGF-BB. n=6. (**F**), Luciferase reporter constructs with full-length *Itga6* promoter were co-transfected with or without TFAP2A and HINT1 plasmid into HEK293T cells, and luciferase activity was evaluated. n=6. (**G**), Luciferase activation driven by the WT *Itga6* promoter or mutant promoter (-1717, -1086, -548, -230, -109 up to +100) normalized to renilla luciferase in HEK293T cells. n=3. (**H**), Identification of HINT1 and TFAP2A interaction in RASMCs by co-immunoprecipitation (immunoprecipitated by HINT1 antibody). (**I**), Confocal fluorescence microscopy of HINT1 (red) and TFAP2A (green) in HASMCs. DAPI, blue; scale bar = 10 and 5μm. (**J**), HEK293T cells were co-transfected with Flag-TFAP2A and HA-HINT1 plasmids. Co-immunoprecipitation analysis of Flag-TFAP2A and HA-HINT1 interaction (immunoprecipitated by HA antibody). (**K**), In vitro binding assay of purified HINT1 and GST-TFAP2A protein (immunoprecipitated by HINT1 antibody). (**L**), Co-immunoprecipitation assay of HINT1 and TFAP2A interaction in HASMCs with PBS or PDGF-BB stimulation for 4h (immunoprecipitated by HINT1 antibody). Statistical analysis was performed by One-way ANOVA for (**B through D, F, G**), Two-way ANOVA for (**E**). For all statistical plots, the data are presented as mean ± SEM.

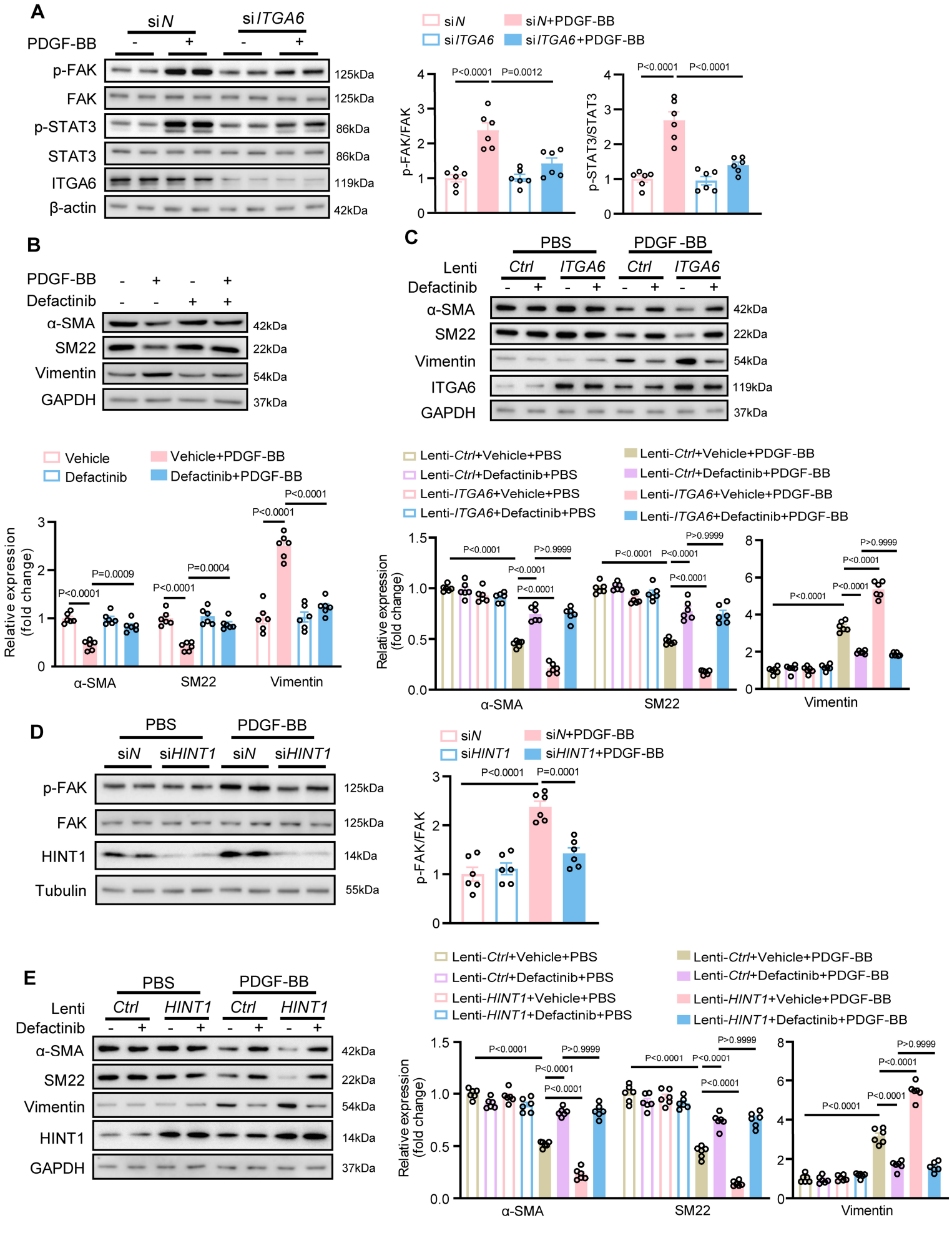
A
siN
siITGA6
PDGF-BB
p-FAK
FAK
p-STAT3
STAT3
ITGA6
β-actin
125kDa
125kDa
86kDa
86kDa
119kDa
42kDa
siN
siN+PDGF-BB
siITGA6
siITGA6+PDGF-BB
P<0.0001
P=0.0012
P<0.0001
P<0.0001
p-FAK/FAK
p-STAT3/STAT3
B
PDGF-BB
Defactinib
α-SMA
SM22
Vimentin
GAPDH
42kDa
22kDa
54kDa
37kDa
C
PBS
PDGF-BB
Lenti
Ctrl
ITGA6
Defactinib
α-SMA
SM22
Vimentin
ITGA6
GAPDH
42kDa
22kDa
54kDa
119kDa
37kDa
Vehicle
Defactinib
Vehicle+PDGF-BB
Defactinib+PDGF-BB
Relative expression (fold change)
P<0.0001
P=0.0009
P<0.0001
P=0.0004
P<0.0001
P<0.0001
α-SMA
SM22
Vimentin
Lenti-Ctrl+Vehicle+PBS
Lenti-Ctrl+Defactinib+PBS
Lenti-ITGA6+Vehicle+PBS
Lenti-ITGA6+Defactinib+PBS
Lenti-Ctrl+Vehicle+PDGF-BB
Lenti-Ctrl+Defactinib+PDGF-BB
Lenti-ITGA6+Vehicle+PDGF-BB
Lenti-ITGA6+Defactinib+PDGF-BB
P<0.0001
P>0.9999
P<0.0001
P<0.0001
P<0.0001
P>0.9999
P<0.0001
P<0.0001
P<0.0001
P>0.9999
P<0.0001
P<0.0001
α-SMA
SM22
Vimentin
D
PBS
PDGF-BB
siN
siHINT1
siN
siHINT1
p-FAK
FAK
HINT1
Tubulin
125kDa
125kDa
14kDa
55kDa
siN
siN+PDGF-BB
siHINT1
siHINT1+PDGF-BB
P<0.0001
P=0.0001
p-FAK/FAK
E
PBS
PDGF-BB
Lenti
Ctrl
HINT1
Defactinib
α-SMA
SM22
Vimentin
HINT1
GAPDH
42kDa
22kDa
54kDa
14kDa
37kDa
Lenti-Ctrl+Vehicle+PBS
Lenti-Ctrl+Defactinib+PBS
Lenti-HINT1+Vehicle+PBS
Lenti-HINT1+Defactinib+PBS
Lenti-Ctrl+Vehicle+PDGF-BB
Lenti-Ctrl+Defactinib+PDGF-BB
Lenti-HINT1+Vehicle+PDGF-BB
Lenti-HINT1+Defactinib+PDGF-BB
Relative expression (fold change)
P<0.0001
P>0.9999
P<0.0001
P<0.0001
P<0.0001
P>0.9999
P<0.0001
P<0.0001
P<0.0001
P>0.9999
P<0.0001
P<0.0001
α-SMA
SM22
Vimentin

Figure 7: ITGA6 aggravates vascular smooth muscle cell phenotypic switching via activating FAK/STAT3 signal pathway.

(**A**), Western blotting analysis of phosphorylation levels of FAK and STAT3 in HASMCs that transfected with si*N* or si*ITGA6* followed by PBS or PDGF-BB (20 ng/ml) stimulation for 30 min. n=6 per group. (**B**), Western blotting analysis of VSMC contractile markers (α-SMA and SM22α) and synthetic markers (Vimentin) in HASMCs pretreated with or without Defactinib (2.5 μM) followed by PBS or PDGF-BB (20 ng/ml) stimulation. n=6 per group. (**C**), Western blotting analysis of VSMC contractile markers (α-SMA and SM22) and synthetic markers (Vimentin) expression in HASMCs infected with Lenti-*Ctrl* or Lenti-*ITGA6* and pretreated with or without Defactinib (2.5 μM) followed by PBS or PDGF-BB (20 ng/ml) stimulation. n=6 per group. (**D**), Western blotting analysis of phosphorylation levels of FAK in HASMCs that transfected with si*N* or si*HINT1* followed by PBS or PDGF-BB (20 ng/ml) stimulation. n=6 per group. (**E**), Western blotting analysis of VSMC contractile markers (α-SMA and SM22) and synthetic markers (Vimentin) expression in HASMCs infected with Lenti-*Ctrl* or Lenti-*HINT1* and pretreated with or without Defactinib (2.5 μM) followed by PBS or PDGF-BB (20 ng/ml) stimulation. n=6 per group. Statistical analysis was performed by One-way ANOVA for (**A , B and D**), Two-way ANOVA for (**C and E**). For all statistical plots, the data are presented as mean ± SEM.

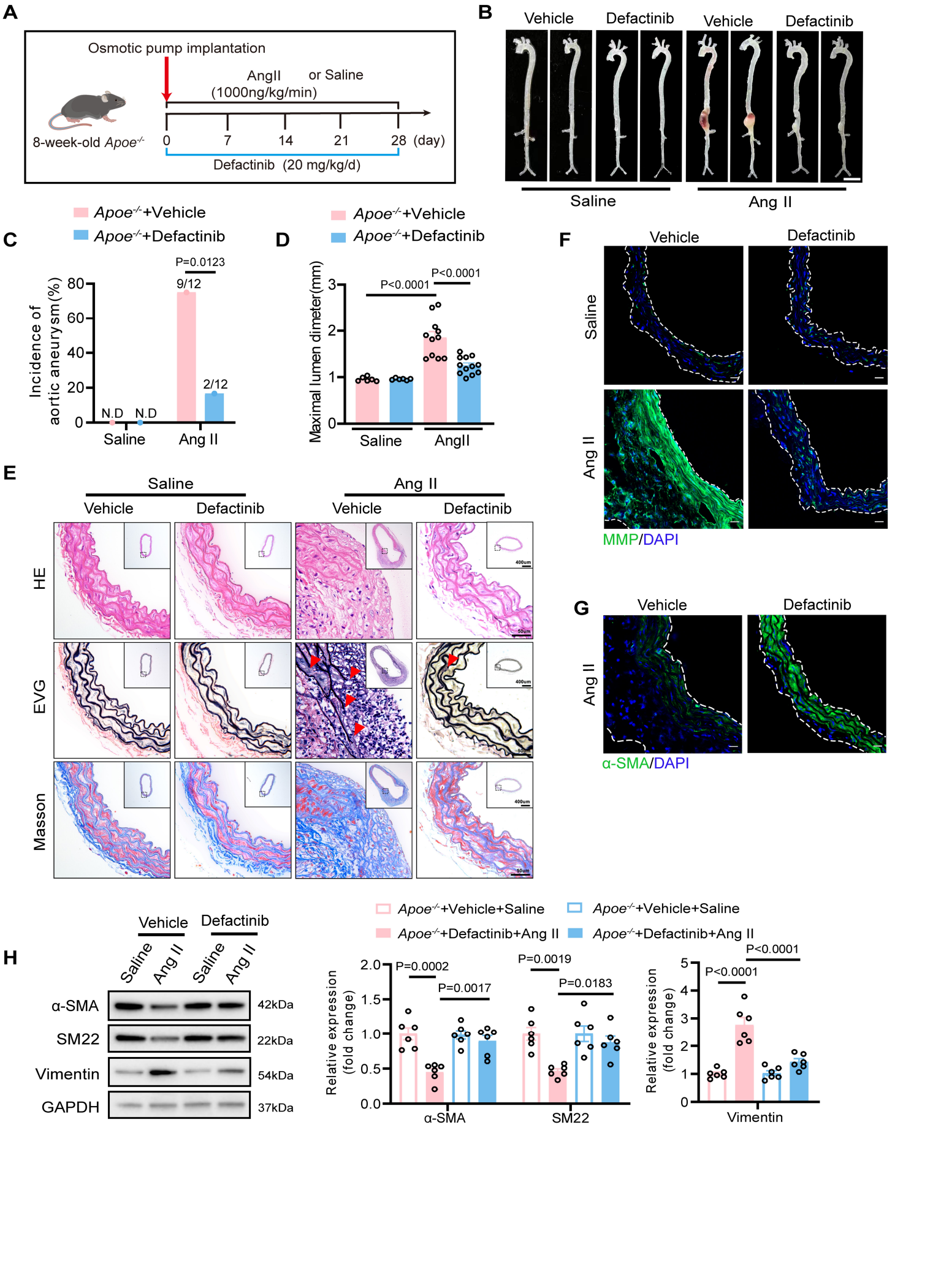
A
Osmotic pump implantation
AngII or Saline
(1000ng/kg/min)
8-week-old Apoe-/-
0 7 14 21 28 (day)
Defactinib (20 mg/kg/d)
B
Vehicle
Defactinib
Vehicle
Defactinib
Saline
Ang II
C
Apoe-/-+Vehicle
Apoe-/-+Defactinib
P=0.0123
9/12
2/12
N.D
N.D
Incidence of aortic aneurysm(%)
Saline
Ang II
D
Apoe-/-+Vehicle
Apoe-/-+Defactinib
P<0.0001
P<0.0001
Maximal lumen dimeter(mm)
Saline
AngII
E
Saline
Ang II
Vehicle
Defactinib
Vehicle
Defactinib
HE
EVG
Masson
F
Vehicle
Defactinib
Saline
Ang II
MMP/DAPI
G
Vehicle
Defactinib
Ang II
α-SMA/DAPI
H
Vehicle
Defactinib
Saline
Ang II
Saline
Ang II
α-SMA
SM22
Vimentin
GAPDH
42kDa
22kDa
54kDa
37kDa
Apoe-/-+Vehicle+Saline
Apoe-/-+Vehicle+Saline
Apoe-/-+Defactinib+Ang II
Apoe-/-+Defactinib+Ang II
Relative expression (fold change)
P=0.0002
P=0.0017
P=0.0019
P=0.0183
α-SMA
SM22
P<0.0001
P<0.0001
Vimentin

Figure 8: Defactinib protects against aortic aneurysm.

(**A**), Eight-week-old male Apoe$^{-/-}$ mice were treated with Defactinib (20 mg/kg/day) daily via intragastric administration, starting at the first day of Ang II infusion and continuing for 28 days. (**B**), Representative photograph of aortas from saline or Ang II-infused *Apoe*$^{-/-}$ mice. (**C**), Incidence of saline or Ang II-induced aortic aneurysm. (**D**), Maximal abdominal lumen diameter of saline (n=6) or Ang II (n=11-12) infused mice measured by ultrasound. (**E**), Histopathological images of suprarenal abdominal aortas of saline or Ang II-infused *Apoe*$^{-/-}$ mice; scale bar = 50 and 400 μm. (**F**), Representative in situ zymography photomicrographs showing matrix metalloproteinase (MMP) activity of suprarenal abdominal aortas; L: Lumen; scale bar = 20 μm. (**G**), Representative immunofluorescence staining of α-SMA expression in suprarenal abdominal aortas; L: Lumen; scale bar = 20 μm. (**H**), Western blotting analysis of the VSMC contractile markers (α-SMA and SM22) and synthetic markers (Vimentin) in suprarenal abdominal aortas from saline or Ang II-infused *Apoe*$^{-/-}$ mice. n=6 per group. Statistical analysis was performed by a Fisher exact test for (**C**), One-way ANOVA for (**D and H**). For all statistical plots, the data are presented as mean ± SEM.